FEDERAL UNIVERSITY OF JUIZ DE FORA

GRADUATE PROGRAM OF CHEMISTRY

MASTER IN CHEMISTRY

Jhonnatan Carvalho de Oliveira Gomes

NMR-DKH BASIS SET ANALYSIS FOR CALCULATION OF $^{1}J(^{195}Pt-^{15}N)$ IN PLATINUM(II) COMPLEXES

Juiz de Fora

2020

Jhonnatan Carvalho de Oliveira Gomes

NMR-DKH BASIS SET ANALYSIS FOR CALCULATION OF $^{1}J(^{195}Pt\text{-}^{15}N)$ IN PLATINUM(II) COMPLEXES

Dissertation presented to the Graduate Program of Chemistry at Federal University of Juiz de Fora as partial requirement to obtain the title of Master in Chemistry. Concentration field: Physical Chemistry.

Advisor: Prof. Dr. Hélio Ferreira dos Santos

Co-advisor: Prof. Dr. Diego Fernando da Silva Paschoal

Juiz de Fora

2020

Ficha catalográfica elaborada através do programa de geração
automática da Biblioteca Universitária da UFJF,
com os dados fornecidos pelo(a) autor(a)

Gomes, Jhonnatan Carvalho de Oliveira.
NMR-DKH basis set analysis for calculation of 1J(195Pt-15N) in platinum(II) complexes / Jhonnatan Carvalho de Oliveira Gomes. -- 2020.
82 f. : il.

Orientador: Hélio Ferreira dos Santos
Coorientador: Diego Fernando da Silva Paschoal
Dissertação (mestrado acadêmico) - Universidade Federal de Juiz de Fora, Instituto de Ciências Exatas. Programa de Pós-Graduação em Química, 2020.

1. RMN. 2. NMR-DKH. 3. DFT. 4. constante de acoplamento 1J(195Pt-15N). 5. complexos de platina(II). I. Santos, Hélio Ferreira dos, orient. II. Paschoal, Diego Fernando da Silva, coorient. III. Títu

Jhonnatan Carvalho de Oliveira Gomes

NMR-DKH basis set analysis for calculation of $^{1}J(^{195}Pt\text{-}^{15}N)$ in platinum(II) complexes

Dissertação apresentada ao Programa de Pós-Graduação em Química da Universidade Federal de Juiz de Fora como requisito parcial à obtenção do título de Mestre em Química. Área de concentração: Físico-Química.

Aprovada em 21 de fevereiro de 2019.

BANCA EXAMINADORA

Prof. Dr. Hélio Ferreira dos Santos - Orientador
Universidade Federal de Juiz de Fora

Prof. Dr. Diego Fernando da Silva Paschoal - Coorientador
Universidade Federal do Rio de Janeiro

Prof. Dr. José Walkimar de Mesquita Carneiro
Universidade Federal Fluminense

Prof. Dr. Alexandre Amaral Leitão
Universidade Federal de Juiz de Fora

I dedicate this work to my eternal friend Victória da Silva Coelho Rapozo (*In Memoriam*), a great friend and an incredible supporter.

ACKNOWLEDGMENTS

First, I would like to thank my advisors Hélio Dos Santos and Diego Paschoal for patience, guidance and inspiration throughout the two years we have worked together in this project. I will certainly carry all your advices and knowledge transmitted in my academical life. I take the opportunity to also thank CAPES, FAPEMIG and CNPq for financial support.

I would also like to thank my mother Simone for always supporting my educational choices, providing me with good education in my life and allowing me to pursue my goals.

My special thanks to my colleagues from my research group NEQC for helping me with my questions and doubts regarding computational chemistry and also for the many great moments we have spent together in the past two years, my sincere gratitude: Nathália Rosa, Julio Arvellos, Rodrigo Fraga, Yulianna Delgado, Maria Eduarda Martins and Ingrid Veríssimo. A special thanks to my friend and colleague Eduardo Almeida, for being a good friend in an unknown environment and for providing me with so many good memories from my master's time.

I also want to express my gratitude towards the people I have met during my stay at UFJF, you all will always be part of this moment: Patrícia BarSan, Pedro Henrique Nascimento, Larissa Albuquerque, Igor Lima, Bruna Neves, Ítalo Monteiro and José Eugênio.

There is also need to thank my friends that have been with me during my educational journey, having my back, helping me in times of need and always showing confidence in me, my most sincere appreciations to: Giuliana Braga, Ana Luísa Pancotti, Dandara Soares, Yasmin Galvão, my fianceé Mariana Trevares, Maria Eduarda Norões, Vitthor Beauclair, Beatriz Lima, Matheus Pires, Derick Braga, Bruno Moynier, Tavinho Souza, Talita Zappala, Izabela Gomes, Mayane Barbosa, Viviane Marquete, Marcela Álvaro, Daniele Crespo, Mariana Nunes, Svenja Gutsche, Julia Ottersbach, Antoine Jourdan, Anaëlle Girard, Julius Späth and Yvonne Florissen.

Tro ikke mørket når lyset går ned i skumringens fang. Alltid er det på jorden et sted soloppgang. (ANDRÉ BJERKE, 1953).

ABSTRACT

The Nuclear Magnetic Resonance is a widely used technique and plays a key role in many different areas, especially in elucidation of reaction mechanisms and designing of new drugs. In this context, the use of Quantum Chemistry methods is an important tool in NMR study. However, theoretical calculations of NMR parameters are, most of the times, expensive and imprecise. Therefore, one of the greatest challenges in Computational Chemistry is developing protocols with low computational cost that yield satisfactory results. In this work, the $^{1}J(^{195}Pt\text{-}^{15}N)$ coupling constant was studied in Pt(II) complexes in order to develop a computational protocol for the calculation of the constant with affordable cost and satisfactory results using the all-electron relativistic basis set NMR-DKH, previously proposed for calculation of ^{195}Pt chemical shift. Several topics were tested and analyzed in order to develop the protocol, such as DFT functionals and modifications to the basis set. The final computational protocol for predicting the $^{1}J(^{195}Pt\text{-}^{15}N)$ coupling constant in Pt(II) complexes included a working set of 82 coupling constants for 57 Pt(II) complexes. Furthermore, it was applied for a testing set of 16 coupling constants in 14 Pt(II) complexes. The protocol was based on nonrelativistic calculations at PBEPBE/NMR-DKH level. The MAD was 36 Hz corresponding to the MRD of 10.4%, considering all 98 coupling constants for 71 Pt(II) complexes.

Keywords: NMR. Pt-195 nucleus. $^{1}J(^{195}Pt\text{-}^{15}N)$ coupling constants. NMR-DKH. DFT. platinum(II) complexes.

RESUMO

A Ressonância Magnética Nuclear é uma técnica amplamente utilizada e tem um papel fundamental em diferentes áreas, especialmente na elucidação de mecanismos reacionais e desenvolvimento de novos fármacos. Neste contexto, o uso de métodos de Química Quântica é uma importante ferramenta no auxílio aos estudos de RMN. No entanto, os cálculos teóricos dos parâmetros de RMN são muitas vezes custosos e imprecisos. Assim, um dos maiores desafios na Química Computacional é desenvolver protocolos com baixo custo computacional que levem a bons resultados. Neste trabalho, a constante de acoplamento $^{1}J(^{195}Pt\text{-}^{15}N)$ foi estudada em complexos de platina(II) a fim de desenvolver um protocolo para o cálculo da constante com custo computacional acessível e resultados satisfatórios, usando a função de base relativística *all-electron* NMR-DKH, previamente desenvolvida para o cálculo do deslocamento químico de ^{195}Pt. Diversos tópicos foram testados e analizados no desenvolvimento do protocolo, como funcionais DFT e modificações na função de base. O protocolo computacional final para o cálculo da constante de acoplamento $^{1}J(^{195}Pt\text{-}^{15}N)$ incluiu um conjunto de 82 constantes de acoplamento para 57 complexos de Pt(II). Ademais, o protocol foi aplicado a um conjunto teste de 16 constantes de acoplamento para 14 complexos de Pt(II). O protocolo foi baseado em cálculos não-relativísticos no nivel PBEPBE/NMR-DKH. O desvio absoluto médio foi de 36 Hz, que corresponde a um desvio relativo médio de 10.4% considerando todas as 98 constantes de acoplamento para os 71 complexos de Pt(II).

Palavras-chave: RMN. núcleo Pt-195. constante de acoplamento $^{1}J(^{195}Pt\text{-}^{15}N)$. NMR-DKH. DFT. complexos de platina(II).

LIST OF FIGURES

LIST OF TABLES

LIST OF ABBREVIATIONS

aiMD	*ab initio* molecular dynamic
DD	dipole-dipole
DFT	Density Functional Theory
DKH	Douglas-Kroll-Hess
DMSO	dimethyl sulfoxide
ECP	effective core potential
erf	error function
erfc	complementary error function
Et	ethyl
FC	Fermi contact
GGA	generalized gradient approximation
GH	global hybrid
GTO	Gaussian-type orbitals
HF	Hartree-Fock
ICF	inhomogeneity correction factor
IEFPCM	integral equation formalism for polarized continuum model
LDA	local density approximation
LSDA	local spin density approximation
MAD	mean absolute deviation
MCDF	multiconfigurational Dirac-Fock
Me	methyl
mGGA	meta-generalized gradient approximation
MRD	mean relative deviation
NMR	nuclear magnetic resonance
Oeimp	(*E*)-2-(((2-oxidoethyl)imino)methyl)phenolate
PCM	polarized continuum model
PES	potential energy surface
Ph	phenyl
RSH	range-separated hybrid
SCRF	self-consisted reaction field
SIE	self-interaction error

SO	spin-orbit
STO	Slater-type orbitals
TZ2P	triple-zeta doubly polarized
tu	thiourea
UEG	uniform electron gas
UHF	unrestricted Hartree-Fock
ZORA	zeroth-order regular approximation

SUMMARY

1 INTRODUCTION

Nuclear magnetic resonance (NMR) spectroscopy is a technique that has been widely studied since 1937, when it was first published by the physician Isidor Isaac Rabi (RABI, 1937). Since then, the technique has been improved and in 1953 the first commercial spectrometer was launched by the Varian brothers. NMR spectroscopy is largely used to help understanding and studying different systems in many areas, such as Chemistry, Physics, Pharmacy, Medicine and Biology. In special, in the chemical and pharmaceutical areas, NMR plays an important role in elucidation of reaction mechanisms as well as in designing of new drugs (VINJE, 2007). Platinum complexes, for instance, are widely used as anticancer drugs where cisplatin (cis-diamminedichloroplatinum(II)) is the most adopted anticancer drug worldwide (GUVEN, 2012). Coupling constant represents the indirect coupling of two nuclei mediated by the bonding electrons between them, therefore, the coupling constant is the spectral manifestation of a chemical bond (STILL, 2007). In Pt(II) complexes, the coupling constant between ^{195}Pt and ^{15}N nuclei ranges from 100 to 700 Hz, varying above and below this range (PREGOSIN, 1982).

One of the greatest challenges in Computational Chemistry is developing protocols with low computational cost that yield satisfactory results. There are not many available works on predicting $^{1}J(^{195}Pt\text{-}^{15}N)$ due to its complexity arisen from heavy nuclei such as Pt. Sutter and coworkers reported the importance of explicit solvation model in calculating $^{1}J(^{195}Pt\text{-}^{15}N)$ with *ab initio* molecular dynamic (aiMD) (SUTTER, 2011). As the authors pointed out, the calculations converged with 12 water molecules as explicit solvent for *cis*-$[Pt(NH_3)_2(OH)_2]$ and *cis*-$[Pt(NH_3)_2Cl_2]$ complexes. They also investigated both hybrid and pure functionals as well as scalar and spin-orbit relativistic effects in the calculation. They concluded that best results were achieved with spin-orbit (SO) ZORA (zeroth-order regular approximation) and hybrid functional (PBE0). This methodology, SO-ZORA/PBE0, was tested for four complexes, *cis*-$[Pt(NH_3)_2(OH)_2]$, *cis*-$[Pt(NH_3)_2Cl_2]$, *cis*-$[Pt(NH_3)_2Br_2]$ and *cis*-$[Pt(NH_3)_2(OH)Cl]$. The results were rather satisfactory with an MRD of 10.6% when compared with experimental data. Although it may produce satisfactory results, the explicit solvation model and aiMD are very expensive and it may become impractical to large systems.

In 2016, our group developed an all-electron relativistic triple-zeta doubly polarized basis set (TZ2P), called NMR-DKH, to calculate the chemical shift (δ) of ^{195}Pt nucleus (PASCHOAL, 2016). The basis set was built by following four steps:

I. Determination of maximum exponents for each angular momentum according to Eq. (1):

$$\propto_l = k_l \frac{2f_l^2}{\pi < r_l >^2} \quad (1)$$

In Eq. (1), l determines the type of the orbital based on the angular momentum ($l = s, p, d, f, ...$), $\propto_l$ is the maximum exponent, $k_l = 1000, 100, 33 \; and \; 10$ for s, p, d and f functions, respectively, $f_l = 1, \frac{4}{3}, \frac{8}{5} \; and \; \frac{64}{35}$ for s, p, d and f functions, respectively, and $< r_l >$ is the innermost radial expected value, and it was obtained for each angular momentum using the multiconfigurational Dirac-Fock (MCDF) numerical calculations for each atom at ground state. The maximum exponents for each atom present in this work is displayed in Table 1.

Table 1. Maximum exponents, $\propto_l$, in Bohr^{-1}, for some atoms used in the development of NMR-DKH basis set

Atom	$\propto_s$	$\propto_p$	$\propto_d$	$\propto_f$
H	282.952156333090	-	-	-
C	8846.12353391750	37.2940933931704	-	-
N	12238.3269689590	54.1425482486954	-	-
O	16178.1182314232	73.8543986696091	-	-
P	59538.0043013517	487.996723151500	-	-
S	68045.9311288506	587.120519822969	-	-
Cl	77142.8171643825	694.985360568515	-	-
As	307826.456351107	3710.76571989537	120.738502480645	-
Br	348670.995115554	4271.50436123164	157.766242822167	-
I	859363.607413965	11648.9850075240	659.513527911096	-
Pt	2164481.60896527	32357.9152575654	1911.90035078584	82.2896809794193

Reference: Adapted from PASCHOAL, *et al*, 2016.

II. Generation of the series of descending primitives according to Eq. (2):

$$\xi_l = \alpha_l \chi^{-i} \quad (2)$$

In Eq. (2), ξ_1 corresponds to the series of primitive for each angular momentum and χ^{-i} is defined for each angular momentum from the respective row in periodic table, shown in Table 2, being i a positive integer.

Table 2. χ values determined for each angular momentum with some rows of the periodic table used in the development of NMR-DKH basis set

Row	χ_s	χ_p	χ_d	χ_f
H-He	3.25	-	-	-
Li-Ne	3.00	3.25	-	-
Na-Ar	2.75	3.00	-	-
Ga-Kr	2.50	2.75	3.00	-
In-Xe	2.25	2.50	2.75	-
Pt	2.00	2.25	2.50	2.75

Reference: Adapted from PASCHOAL, *et al*, 2016.

III. Contraction of basis set with a triple-zeta scheme. The contraction was made only to the first function for each angular momentum. The contraction coefficients were obtained at unrestricted Hartree-Fock (UHF) level with Douglas-Kroll-Hess second-order scalar relativistic correction (DKH_2).

IV. Addition of two polarization functions. The exponents of such functions were modified in order to minimize the energy at UHF-DKH level.

The scheme contraction and the number of functions are both presented in Table 3.

Table 3. Relativistic atomic basis set NMR-DKH

Atoms	Contraction Scheme	GTO	CGTO
H-He	(7s2p) → [3s2p]	13	9
Li-Ne	(11s6p2d) → [6s3p2d]	39	25
Na-Ar	(15s10p2d) → [9s6p2d]	55	37
Ga-Kr	(18s13p6d2f) → [12s9p3d2f]	101	68
In-Xe	(22s16p6d2f) → [15s12p6d2f]	129	95
Pt	(26s18p13d6f2g) → [18s12p9d3f2g]	203	136

Reference: Adapted from PASCHOAL, *et al*, 2016.

An scaling model was proposed by fitting ^{195}Pt chemical shift for a set of 183 Pt(II) complexes, with the shielding constants (σ) calculated at density functional level (DFT) using the non-relativistic protocol PBEPBE/NMR-DKH/IEFPCM(UFF)//B3LYP/LANL2DZ/Def2-SVP/IEFPCM(UFF). The MAD (mean absolute deviation) and the MRD (mean relative deviation) were 168 ppm and 5%, respectively. Although the NMR-DKH basis set proved satisfactory at predicting the ^{195}Pt chemical shift, the coupling constant is a far more sensitive NMR property. With this in mind, in this work the $^{1}J(^{195}Pt\text{-}^{15}N)$ coupling constant was studied in Pt(II) complexes in order to develop a computational protocol capable of satisfactorily predict this property using the NMR-DKH basis set. By achieving a low-cost computational protocol, the results may help experimentalists in interpreting Pt(II) NMR spectra, providing valuable information such as distinction between *cis* and *trans* isomers.

2 OBJECTIVES

The general objectives of this work consisted in testing and analyzing the NMR-DKH basis set, already developed, for the calculation of the $^{1}J(^{195}Pt\text{-}^{15}N)$ coupling constant.

2.1 SPECIFIC OBJECTIVES

- Test the relativistic basis set NMR-DKH, developed for the calculation of the chemical shift of the nuclide ^{195}Pt, for the calculation of the $^{1}J(^{195}Pt\text{-}^{15}N)$ coupling constant;
- In case of unsatisfactory results, evaluate the protocol and promote adjustments on the basis set and changes on the level of theory or the used method.

3 COMPUTATIONAL DETAILS

In this section, the computational details will be presented.

3.1 STEP 1

Nonrelativistic calculations were performed in the Gaussian 09 software Revision D.01(FRISCH, *et al*, 2009). 67 Pt(II) complexes with at least one Pt-N bond and experimental data for $^{1}J(^{195}Pt\text{-}^{15}N)$ were randomly chosen. All the 67 complexes were built using the software GaussView 5.0.9(FRISCH, *et al*, 2009) and their geometries were optimized and characterized as minimum on the potential energy surface (PES) through harmonic frequency calculations at B3LYP (BECK, 1993; LEE, *et al*, 1988; STEPHENS, *et al*, 1994) level with def2-SVP (WEIGEND & AHLRICHS, 2005) basis set for ligand atoms and LANL2DZ (HAY & WADT, 1985; HAY & WADT, 1985) effective core potential (ECP) for Pt atom. The solvent effect was considered in both optimization and NMR calculations through the self-consisted reaction field (SCRF) method with integral equation formalism for polarized continuum method (IEFPCM) (SCALMANI & FRISCH, 2010). Afterwards, the NMR properties calculations were obtained at PBEPBE (PERDEW, *et al*, 1996; PERDEW, *et al*, 1997) level with the all-electron relativistic basis set NMR-DKH (PASCHOAL, *et al*, 2016) for all atoms. Both optimization and NMR properties calculation levels were chosen based on the work from Paschoal and coworkers (PASCHOAL, *et al*, 2016) for predicting ^{195}Pt NMR chemical shift and can be denoted as PBEPBENMR-DKHIEFPCM(UFF)//B3LYP/LANL2DZ/def2-SVP/IEFPCM (UFF), TEST0.

3.2 STEP 2

From the results obtained in 3.1, four complexes were randomly chosen (see Fig. 1). These complexes were used in a set of tests (TEST1-21) where methodology was changed from TEST0 with purpose of improving the results, aiming for a methodology that provides reliable and satisfactory outcomes. This set of tests was divided into four different categories: NMR-DKH basis set modifications; functional changes; basis set variations; and ligand analysis. In all subsequent tests, the same implicit solvation method as in TEST0 was adopted.

3.2.1 NMR-DKH basis set modifications

A series of modifications was performed in the NMR-DKH basis set:

Figure 1. Test set of complexes used on TEST1-21

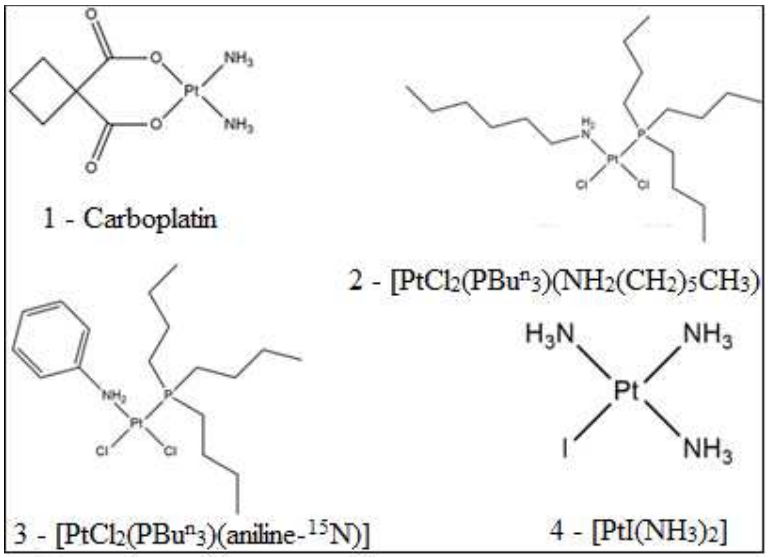

Reference: Own Author.

- Decontraction of all functions and addition of two s functions with high exponent for all atoms, excluding hydrogen, for calculation of J^{FC} contribution; hydrogen atoms had four s functions added – TEST1.
- Decontraction of s function for Pt atom – TEST2;
- Decontraction of s and p functions for Pt atom – TEST3;
- Addition of diffuse functions for all atoms – TEST4;
- Same as TEST1 but with addition of one p function with high exponent for all atoms of diffuse functions for all atoms – TEST5.

The modifications described in TEST1 were made automatically by the use of the keyword *mixed*. The exponents of the s functions for all atoms were calculated from the highest exponent presented in the respective basis set. The exponent for the first and second periods were multiplied by a factor of 3, while for the atoms from third period and on the exponents were multiplied by a factor of 2. The exponents of the added s functions for all atoms, within the test set, are displayed in Table 4. These modifications, though, were only made for the

calculation of the FC contribution. The three remaining contributions were calculated with the original basis set.

As for TEST2 and TEST3, the respective decontractions were made manually. The diffuse functions added in TEST4 were obtained from the equation that generates the series of primitives of the NMR-DKH basis set. The next primitive function series was added for each angular momentum. Regarding the TEST5, the same approach as TEST1 was employed, with the exception that one p function with high exponent was manually added to the basis set. The high exponent was calculated accordingly to the s function: three times higher than the existing higher exponent for first and second periods and twice higher for the third period and on. It is valid to highlight that in TEST5 the p function added was present in calculation of all four contributions, whereas the extra s functions were present only in the calculation of the FC contribution. The p functions exponents are presented in Table 5.

The Table 6 summarizes all modifications made in the NMR-DKH basis set throughout all five initial tests.

Table 4. Exponents of s functions added for calculation of J^{FC} on complexes 1-4

Atom	Exponent 1	Exponent 2	Exponent 3	Exponent 4
Pt	4328963.218	8657926.436	-	-
N	36714.98091	110144.9427	-	-
C	26538.37060	79615.11181	-	-
H	848.8564690	2546.569407	7639.708221	22919.12466
O	48534.35469	145603.0641	-	-
Cl	154285.6343	308571.2687	-	-
P	119076.0086	238152.0172	-	-
I	1718727.215	3437454.430	-	-

Reference: Own Author.

Table 5. Exponents of p functions added for calculation of J on complexes 1-4

Atom	Exponent
Pt	64715.830515131
N	162.427644746
C	111.88228018
H	2.6445
O	221.563196009
Cl	2084.956081706
P	1463.990169454
I	23297.970015048

Reference: Own Author.

Table 6. NMR-DKH basis set modifications on TEST1-5

Atom	NMR-DKH	TEST1	TEST2	TEST3	TEST4	TEST5
Pt	[18s12p9d3f2g]	(28s18p13d6f2g)	[26s12p9d3f2g]	[26s18p9d3f2g]	[19s13p10d4f2g]	(28s19p13d6f2g)
N	[6s3p2d]	(13s6p2d)	[6s3p2d]	[6s3p2d]	[7s4p2d]	(13s7p2d)
C	[6s3p2d]	(13s6p2d)	[6s3p2d]	[6s3p2d]	[7s4p2d]	(13s7p2d)
H	[3s2p]	(11s2p)	[3s2p]	[3s2p]	[4s2p]	(11s3p)
O	[6s3p2d]	(13s6p2d)	[6s3p2d]	[6s3p2d]	[7s4p2d]	(13s7p2d)
Cl	[9s6p2d]	(17s10p2d)	[9s6p2d]	[9s6p2d]	[10s7p2d]	(17s11p2d)
P	[9s6p2d]	(17s10p2d)	[9s6p2d]	[9s6p2d]	[10s7p2d]	(17s11p2d)
I	[15s12p6d2f]	(24s16p9d2f)	[15s12p6d2f]	[15s12p6d2f]	[16s13p7d2f]	(24s17p9d2f)

Reference: Own Author.

3.2.2 Functional changes

In order to evaluate the importance of DFT functional, ten different functionals were tested in the calculation of the $^{1}J(^{195}Pt\text{-}^{15}N)$ coupling constant. During this set of tests, the NMR-DKH was employed with no modifications. The ten functionals tested were as following:

- B3LYP – TEST6 (BECK, 1993; LEE, *et al*, 1988; STEPHENS, *et al*, 1994);
- TPSSh – TEST7 (TAO, *et al*, 2003; STAROVEROV, *et al*, 2003);
- M06-2X - TEST8 (ZHAO, *et al*, 2008);
- M06 – TEST9 (ZHAO, *et al*, 2008);
- CAM-B3LYP – TEST10 (YANAI, *et al*, 2004);

- LC-ωPBE – TEST11 (HENDERSON, *et al*, 2009; VYDROV, *et al*, 2006; VYDROV, *et al*, 2006; VYDROV, *et al*, 2007);
- LC-BLYP – TEST12 (IIKURA, *et al*, 2001);
- BB95 – TEST13 (BECKE, 1996);
- mPW1PW91 – TEST14 (ADAMO, *et al*, 1998);
- PBE1PBE – TEST15 (ADAMO, *et al*, 1999; ERNZERHOF, *et al*, 1999).

3.2.3 Basis set variation

Some basis set were tested in the calculation of $^{1}J(^{195}Pt\text{-}^{15}N)$ coupling constant. There were tested different basis sets for either the metal as well as the ligands. The aim of these tests was evaluating the results obtained when using NMR-DKH basis set and, also, the importance of the ligand basis set. In this series of tests, the functional PBEPBE was employed in all calculations, varying only the basis set itself, as presented following:

- DZP-DKH basis set for both metal and ligand atoms – TEST16 (BERREDO, *et al*, 2010);
- SAPPORO-DZP-2012 basis set for ligand atoms and SAPPORO-DKH3-DZP-2012 for metal – TEST17 (NORO, *et al*, 2013);
- SAPPORO-TZP-2012 basis set for ligand atoms and SAPPORO-DKH3-DZP-2012 for metal – TEST18 (NORO, *et al*, 2013);
- cc-pVTZ basis set for ligands and NMR-DKH basis set for metal – TEST19 (DUNNING, 1989; KENDALL, *et al*, 1992; WOON, *et al*, 1993; PETERSON, *et al*, 1994; WILSON, *et al*, 1996; DAVIDSON, 1996);
- DZP basis set for ligands and NMR-DKH basis set for metal – TEST20 (DUNNING, 1970);
- TZP basis set for ligands and NMR-DKH basis set for metal – TEST21 (DUNNING, 1971; BINNING, *et al*, 1990; MCLEAN, *et al*, 1980).

3.2.4 Ligand analysis

In this last set of tests, some ligand and ligand-metal interactions were studied. At a total, three different analysis were made:

- Conformational analysis of butyl and hexyl groups in ligands – TEST22;
- Bulky ligand exchange for small ligands – TEST23;
- Pt-N bond length study – TEST24.

In TEST22, the many possible stable conformation states of butyl and hexyl groups were studied in the $[PtCl_2(PBu^n_3)(NH_2(CH_2)_5CH_3)]$ complex. At a total, sixteen different conformations were optimized and their respective $^1J(^{195}Pt\text{-}^{15}N)$ coupling constants were calculated for each conformation, with the TEST0 protocol. The dihedrals and their respective angles are presented in Fig. 2 and Table 7. The purpose of this analysis is to investigate the influence of the conformational structure of the ligands in the calculation of the coupling constant in question.

As for TEST24, the influence of the bulkiness of ligands in the calculation of the $^1J(^{195}Pt\text{-}^{15}N)$ coupling constant was analyzed. Four complexes with bulky phosphine and arsine ligands were randomly chosen and the alkyl group in the ligands were substituted by hydrogens.

The last test, TEST23, consisted in three analysis made by varying the Pt-N bond length in $[Pt(NH_3)_2Cl_2]$ complex in three different intervals: 0.001Å, 0.01Å and 0.1Å. These variations were performed ten times for each interval above and below the optimized bond length.

Figure 2. Dihedrals taken on conformational analysis of $[PtCl_2(PBu^n_3)(NH_2(CH_2)_5CH_3)]$ complex

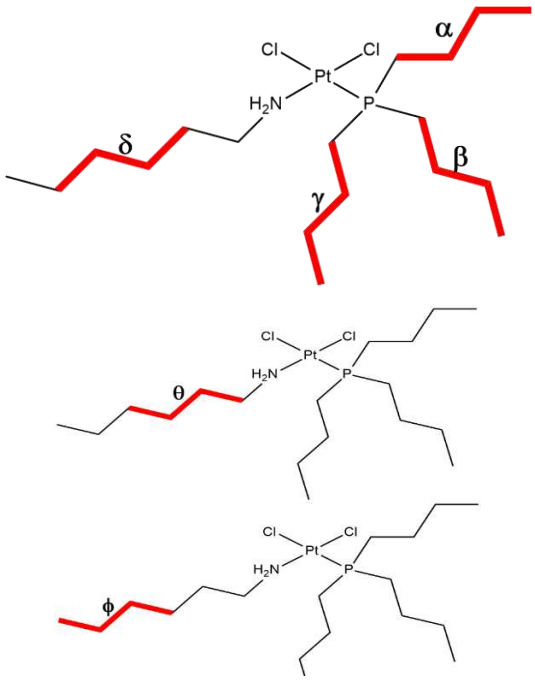

Reference: Own Author.

Table 7. Dihedral angles analyzed on conformational analysis of $[PtCl_2(PBu^n_3)(NH_2(CH_2)_5CH_3)]$ complex

Conformation	α	β	γ	δ	θ	ϕ
I	180.000	180.000	180.000	180.000	180.000	180.000
II	180.000	60.000	180.000	180.000	180.000	180.000
III	180.000	180.000	60.000	180.000	180.000	180.000
IV	180.000	180.000	180.000	60.000	180.000	180.000
V	180.000	60.000	60.000	180.000	180.000	180.000
VI	180.000	60.000	180.000	60.000	180.000	180.000
VII	180.000	180.000	60.000	60.000	180.000	180.000
VIII	180.000	60.000	60.000	60.000	180.000	180.000
IX	60.000	180.000	180.000	180.000	180.000	180.000
X	60.000	60.000	180.000	180.000	180.000	180.000
XI	60.000	180.000	60.000	180.000	180.000	180.000
XII	60.000	180.000	180.000	60.000	180.000	180.000
XIII	60.000	60.000	60.000	180.000	180.000	180.000
XIV	60.000	180.000	60.000	60.000	180.000	180.000
XV	60.000	60.000	180.000	60.000	180.000	180.000
XVI	60.000	60.000	60.000	60.000	180.000	180.000
TEST0	178.304	58.684	-61.451	151.802	22.154	30.179

Reference: Own Author.

3.3 STEP 3

Based on the results obtained in all tests described in 3.2, a new calculation was run for all 68 complexes, giving rise to a new protocol: M06/NMR-DKH+mixed/IEFPCM(UFF)// B3LYP/LANL2DZ/def2-SVP/IEFPCM(UFF). The new protocol can, thus, be compared with the original one proposed, TEST0, making possible to conclude whether the modifications made in 3.3 to the protocol are, in fact, effective.

3.4 STEP 4

The underestimated coupling constants were corrected by two scaling methods. The methods chosen were: (a) mean relative error method, developed by Dos Santos and coworkers (DOS SANTOS, *et al*, 1995) and (b) least squares method.

(a) Mean Relative Error (model 1)

The mean relative error method intends to find a factor that scales the calculated data to approximate it to the experimental data. This factor, S, is given by means of the mean relative error as presented in Eq. (3).

$$S = 1 + \frac{\bar{E}\%}{100 - \bar{E}\%} \tag{3}$$

where $\bar{E}\%$ is the mean relative error from the set of data:

$$\bar{E}\% = \frac{1}{N}\sum_{i=1}^{N}\left|\frac{{}^{1}J_i^{expt.} - {}^{1}J_i^{calc.}}{{}^{1}J_i^{expt.}}\right| \times 100 \tag{4}$$

So, the corrected coupling constant is calculated according to Eq. (5)

$${}^{1}J_i^{scal.-1} = S\,{}^{1}J_i^{calc.} \tag{5}$$

where ${}^{1}J_i^{calc.}$ is the coupling constant obtained with the methodology employed in TEST0.

(b) Least Squares Method (model 2)

In the second approach, labelled as Model 2, a standard linear correlation was used with the coupling constants calculated as:

$${}^{1}J_i^{scal.-2} = a\,{}^{1}J_i^{calc.} + b \tag{6}$$

In both scaling procedures, a set of 82 coupling constants from 57 Pt(II) complexes was used to fit the models, and an additional set of 16 coupling constants from 14 Pt(II) complexes to validate them.

4 RESULTS AND DISCUSSION

In this section, all the results will be presented and discussed.

4.1 STEP 1

From the 67 Pt(II) complexes selected, a total of 92 different coupling constants, $^{1}J(^{195}Pt\text{-}^{15}N)$ were calculated. The values for all the 92 coupling constants are displayed in Table 8, alongside with the respective experimental data. It is worth mentioning that all coupling constants obtained theoretically were negative whereas the experimental data are given as positive values. Indeed, the one-bond coupling constant, ^{1}J, is negative if the gyromagnetic ratios of the bonding atoms have opposite signs. Since the gyromagnetic ratio of the ^{195}Pt nucleus is $\gamma = 5.768 \times 10^{7} rad \cdot T^{-1} \cdot s^{-1}$ and the gyromagnetic ratio of the ^{15}N nucleus is $\gamma = -2.713 \times 10^{7} rad \cdot T^{-1} \cdot s^{-1}$ the one bond coupling constant between these two nuclei will be negative (LEVITT, 2008). Therefore, for terms of comparison, the theoretical coupling constant will be taken as positive in this work. Analyzing the $^{1}J(^{195}Pt\text{-}^{15}N)$ in Table 8, it becomes clear that the level of theory chosen underestimate most of the coupling constants (82 out of 92), overestimating only 10 coupling constants. The protocol was capable of sufficiently predicting only one coupling constant, in cis-$[Pt(NH_3)_2(NO_2)_2]$ complex, where experimental data is 286 Hz and the calculated 283 Hz, giving a deviation of only 3 Hz and an error of approximately 1%. The mean absolute deviation (MAD) of the calculated coupling constant was 105 Hz while the mean relative deviation (MRD) was 34.1%. The nitro groups (**$[Pt(NO_2)_3X]$** and **$[Pt(NO_2)_2X_2]$**) presented the largest deviation (around 200 Hz), whilst groups **$[Pt(NCS)_2X_2]$** and **[Pt(N-hexyl)X_2Y]** presented the lowest (around 55 Hz). The three amino groups presented very similar deviation. Fig. 3 and Fig. 4 showcase this underestimation clearer. Whereas experimental values range from 103 to 754 Hz, the theoretical ones range from 99 to 571 Hz (not necessarily corresponding to one another). Most coupling constants lies in the interval 150-250 Hz and 250-350 Hz for the theoretical and experimental data, respectively. It is evident in Fig. 4 that the behavior of the calculated coupling constants compared to the experimental data is very consistent throughout the series of complexes presented. These results show that even though the methodology applied underestimates most of the coupling constant, the error within the values is systematical.

The 10 complexes that presented overestimated coupling constant all contain bulky phosphine/arsine ligands, arising suspicion that these voluminous groups may influence in the overestimation of the coupling constant. This will be further discussed in section 4.2.

Table 8. Calculated $^{1}J(^{195}Pt–^{15}N)$ ($^{1}J_{i}^{calc.}$ in Hz) for the set of 94 coupling constants in 69 Pt(II) complexes at PBEPBE/NMR-DKH/IEFPCM(UFF)//B3LYP/LANL2DZ/def2-SVP/IEFPCM(UFF) level with their respective experimental data

Pt(II) Complexes	Solvent	OBS[a]	$^{1}J_{i}^{calc.}$ [b]	Expt.
[Pt(NH$_3$)$_3$X]				
[Pt(NH$_3$)$_4$]$^{2+}$	H$_2$O		194	287[c]
[Pt(NH$_3$)$_3$(DMSO)]	DMSO	*trans* to NH$_3$	204	288[d]
[Pt(NH$_3$)$_3$(DMSO)]	DMSO	*trans* to DMSO	202	232[d]
[Pt(NH$_3$)$_3$Cl]$^{+}$	DMSO	*trans* to Cl^{-}	219	317[d]
[Pt(NH3)$_3$Cl]$^{+}$	DMSO	*trans* to NH$_3$	172	278[d]
[Pt(NH$_3$)$_3$(H$_2$O)]$^{2+}$	H$_2$O	*trans* to H$_2$O	292	376[e]
[Pt(NH$_3$)$_3$(H$_2$O)]$^{2+}$	H$_2$O	*cis* to H$_2$O	178	299[e]
[Pt(NH$_3$)$_3$(OH)]$^{+}$	H$_2$O	*trans* to OH^{-}	150	286[e]
[Pt(NH$_3$)$_3$(OH)]$^{+}$	H$_2$O	*cis* to OH^{-}	200	294[e]
[Pt(NH$_3$)$_3$(OSO$_3$)]	H$_2$O	*trans* to OSO$_3^{2-}$	190	362[e]
[Pt(NH$_3$)$_3$(OSO$_3$)]	H$_2$O	*cis* to OSO$_3^{2-}$	194	303[e]
[PtCl(NH$_3$)$_3$]$^{+}$	H$_2$O	*trans* to Cl^{-}	221	331[e]
[PtCl(NH$_3$)$_3$]$^{+}$	H$_2$O	*cis* to Cl^{-}	172	281[e]
[PtBr(NH$_3$)$_3$]$^{+}$	H$_2$O	*trans* to Br^{-}	214	319[e]
[PtBr(NH$_3$)$_3$]$^{+}$	H$_2$O	*cis* to Br^{-}	168	276[e]
[PtI(NH$_3$)$_3$]$^{+}$	H$_2$O	*trans* to I^{-}	205	289[e]
[PtI(NH$_3$)$_3$]$^{+}$	H$_2$O	*cis* to I^{-}	164	269[e]
[Pt(NH$_3$)$_3$(NO$_2$)]	H$_2$O	*trans* to NO^{2-}	148	254[e]
[Pt(NH$_3$)$_3$(NO$_2$)]	H$_2$O	*cis* to NO^{2-}	238	319[e]
[Pt(NH$_3$)$_3$(DMSO)]$^{2+}$	H$_2$O	*trans* to DMSO	202	243[e]
[Pt(NH$_3$)$_3$(DMSO)]$^{2+}$	H$_2$O	*cis* to DMSO	204	303[e]
[Pt(NH$_3$)$_3$(tu)]$^{2+}$	H$_2$O	*trans* to tu	177	243[e]
[Pt(NH$_3$)$_3$(tu)]$^{2+}$	H$_2$O	*cis* to tu	178	277[e]
[Pt(NH$_3$)$_3$(SCN)]$^{+}$	H$_2$O	*trans* to SCN^{-}	186	264[e]
[Pt(NH$_3$)$_3$(SCN)]$^{+}$	H$_2$O	*cis* to SCN^{-}	177	282[e]
[Pt(NH$_3$)$_2$XY]				
[Pt(NH$_3$)$_2$(CBDCA)]	H$_2$O		212	360[d]
cis-[Pt(NH$_3$)$_2$Cl$_2$]	DMSO		196	312[d]
trans-[Pt(NH$_3$)$_2$Cl(DMSO)]$^{+}$	DMSO	*trans* to NH$_3$	188	287[d]

(Continued)

Table 8. Continued

Pt(II) Complexes	Solvent	OBS[a]	$^1J_i^{calc.}$ [b]	Expt.
cis-$[Pt(NH_3)_2Cl(DMSO)]^+$	DMSO	*trans* to Cl^-	232	340[d]
cis-$[Pt(NH_3)_2Cl(DMSO)]^+$	DMSO	*trans* to DMSO	164	234[d]
cis-$[Pt(NH_3)_2(OH)_2]$	H_2O	*trans* to OH^-	157	293[e]
cis-$[Pt(NH_3)_2(H_2O)(OSO_3)]$	H_2O	*trans* to OSO_3^{2-}	201	374[e]
cis-$[Pt(NH_3)_2(H_2O)(OSO_3)]$	H_2O	*trans* to H_2O	256	392[e]
cis-$[PtCl(H_2O)(NH_3)_2]^+$	H_2O	*trans* to Cl^-	209	343[e]
cis-$[PtCl(H_2O)(NH_3)_2]^+$	H_2O	*trans* to H_2O	258	370[e]
cis-$[PtCl(NH_3)_2(OH)]$	H_2O	*trans* to Cl^-	255	338[e]
cis-$[PtCl(NH_3)_2(OH)]$	H_2O	*trans* to OH^-	140	280[e]
cis-$[PtBr_2(NH_3)_2]$	H_2O	*trans* to Br^-	190	308[e]
cis-$[PtBr(H_2O)(NH_3)_2]^+$	H_2O	*trans* to Br^-	204	331[e]
cis-$[PtBr(H_2O)(NH_3)_2]^+$	H_2O	*trans* to H_2O	253	365[e]
cis-$[PtBr(NH_3)_2(OH)]$	H_2O	*trans* to Br^-	251	326[e]
cis-$[PtBr(NH_3)_2(OH)]$	H_2O	*trans* to OH^-	139	275[e]
cis-$[PtI_2(NH_3)_2]$	H_2O	*trans* to I^-	179	271[e]
cis-$[PtI(H_2O)(NH_3)_2]^+$	H_2O	*trans* to I^-	194	301[e]
cis-$[PtI(H_2O)(NH_3)_2]^+$	H_2O	*trans* to H_2O	246	358[e]
cis-$[Pt(NH_3)_2(NO_2)_2]$	H_2O	*trans* to NO^{2-}	283	286[e]
cis-$[Pt(H_2O)(NH_3)_2(NO_2)]^+$	H_2O	*trans* to NO^{2-}	158	266[e]
cis-$[Pt(H_2O)(NH_3)_2(NO_2)]^+$	H_2O	*trans* to H_2O	338	408[e]
cis-$[Pt(NH_3)_2(SCN)_2]$	H_2O	*trans* to SCN^-	192	259[e]
cis-$[Pt(H_2O)(NH_3)_2(DMSO)]^{2+}$	H_2O	*trans* to DMSO	99	255[e]
cis-$[Pt(H_2O)(NH_3)_2(DMSO)]^{2+}$	H_2O	*trans* to H_2O	214	392[e]
cis-$[Pt(NH_3)_2(tu)_2]$	H_2O	*trans* to tu	170	233[e]
cis-$[Pt(NH_3)_2(DMSO)_2]^{2+}$	DMSO	*trans* to DMSO	196	268[f]
cis-$[Pt(NH_3)_2(DMSO)Br]^+$	DMSO	*trans* to Br^-	245	341[f]
cis-$[Pt(NH_3)_2(DMSO)Br]^+$	DMSO	*trans* to DMSO	170	232[f]
trans-$[Pt(NH_3)_2(DMSO)Br]^+$	DMSO	*trans* to NH_3	183	284[f]
$[Pt(NH_3)X_2Y]$				
cis-$[Pt(NH_3)Cl_2(DMSO)]$	DMSO	*trans* to Cl^-	234	336[d]
trans-$[Pt(NH_3)Cl_2(DMSO)]$	DMSO	*trans* to DMSO	154	232[d]
cis-$[Pt(NH_3)(DMSO)_2(H_2O)]^{2+}$	DMSO	*trans* to DMSO	196	274[f]
cis-$[Pt(NH_3)(DMSO)_2Cl]^+$	DMSO	*trans* to DMSO	222	268[f]
trans-$[Pt(NH_3)(DMSO)(H_2O)_2]^{2+}$	DMSO	*trans* to DMSO	156	256[f]
cis-$[Pt(NH_3)(DMSO)_2Br]^+$	DMSO	*trans* to DMSO	177	268[f]
cis-$[Pt(NH_3)(DMSO)Br_2]$	DMSO	*trans* to Br^-	200	335[f]
trans-$[Pt(NH_3)(DMSO)Br_2]$	DMSO	*trans* to DMSO	150	226[f]

(Continued)

Table 8. Continued

Pt(II) Complexes	Solvent	OBS[a]	$^{1}J_{i}^{calc.}$ [b]	Expt.
$[Pt(NO_2)_3X]$				
$[Pt(NO_2)_4]^{2-}$	H_2O	*trans* to NO^{2-}	368	594[g]
$[Pt(H_2O)(NO_2)_3]^-$	H_2O	*trans* to NO^{2-}	328	531[g]
$[Pt(H_2O)(NO_2)_3]^-$	H_2O	*trans* to H_2O	571	754[g]
$[Pt(NO_2)_3(OH)]^{2-}$	H_2O	*trans* to NO^{2-}	360	583[g]
$[Pt(NO_2)_3(OH)]^{2-}$	H_2O	*trans* to H_2O	358	626[g]
$[Pt(NO_2)_2X_2]$				
cis-$[Pt(H_2O)_2(NO_2)_2]$	H_2O	*trans* to H_2O	468	679[g]
trans-$[Pt(H_2O)_2(NO_2)_2]$	H_2O	*trans* to NO^{2-}	201	470[g]
$[Pt(NCS)_2X_2]$				
cis-$[Pt(CNS)_2(PMe_2Et)_2]$	$(CD_3)_2SO$	Isomer NS	264	205[h]
cis-$[Pt(CNS)_2(PMe_2Et)_2]$	$(CD_3)_2SO$	Isomer NN	264	220[h]
cis-$[Pt(CNS)_2(PEt_3)_2]$	CH_2Cl_2	Isomer NS	290	245[h]
cis-$[Pt(CNS)_2(PEt3)_2]$	CH_2Cl_2	Isomer NN	268	220[h]
$[Pt(N\text{-}hexyl)X_2Y]$				
$[PtCl_2(AsMePh_2)(NH_2(CH_2)_5CH_3)]$	$CDCl_3$		190	209[i]
$[PtCl_2(NH_2(CH_2)_5CH_3)_2]$	$CDCl_3$		196	287[i]
$[PtCl_2(C_2H_4)(NH_2(CH_2)_5CH_3)]$	$CDCl_3$		171	284[i]
$[PtCl_2(PBu^n_3)(NH_2(CH_2)_5CH_3)]$	$CDCl_3$		218	138.3[i]
$[PtCl_2(PMePh_2)(NH_2(CH_2)_5CH_3)]$	$CDCl_3$		205	155.9[i]
$[PtCl_2(AsBu^n_3)(NH_2(CH_2)_5CH_3)]$	$CDCl_3$		203	183.8[i]
Unsorted				
$[Pt(en)(H_2O)_2]^{2+}$	H_2O		281	411[d]
cis-$[PtCl_2(Gly)]^-$	DMSO	*trans* to Cl^-	173	317[d]
trans-$[PtCl_2(Gly)(DMSO)]$	DMSO	*trans* to DMSO	164	244[d]
[Pt(Cl(Gly)(DMSO)] (O-gly *trans* to Cl)	DMSO	*trans* to DMSO	147	226[d]
[PtCl(Gly)(DMSO)] (N-gly *trans* to Cl)	DMSO	*trans* to Cl^-	218	330[d]
$[Pt(en)(DMSO)I]^+$	DMSO	*trans* to I^-	231	345[f]
$[Pt(en)(DMSO)I]^+$	DMSO	*trans* to DMSO	168	247[f]
$[Pt(en)(DMSO)_2]^{2+}$	DMSO	*trans* to DMSO	211	292[f]
$[PtCl_2(PBu^n_3)(t\text{-}Bu(N{=}CH_2)]$	CD_2Cl_2		307	217[j]
$[PtCl_2(PBu^n_3)(aniline)]$	$CDCl_3$		197	103[j]
$[PtCl_2(PBu^n_3)(t\text{-}butylamine)$	$CDCl_3$		226	159[j]
		MAD	**105 Hz**	
		MRD	**34.1%**	

[a] Observation: position of ^{15}N atom coupling with ^{195}Pt; [b] Calculated values at PBEPBE/NMR-DKH/IEFPCM(UFF)//B3LYP/LANL2DZ/def2-SVP/IEFPCM(UFF) protocol; [c] LEVASON, *et al*, 1993; [d] STILL, *et al*, 2007; [e] APPELTON, *et al*, 1986; [f] KERRISON, *et al*, 1985; [g] WOOD, *et al*, 1983; [h] ANDERSON, *et al*, 1976; [i] MOTSCHI, *et al*, 1979; [j] POEL, *et al*, 1981. Reference: Own Author.

Figure 3. Distribution of experimental and theoretical $^{1}J(^{195}Pt\text{-}^{15}N)$ at PBEPBE/NMR-DKH/IEFPCM(UFF)//B3LYP/LANL2DZ/def2-SVP/IEFPCM(UFF) level.

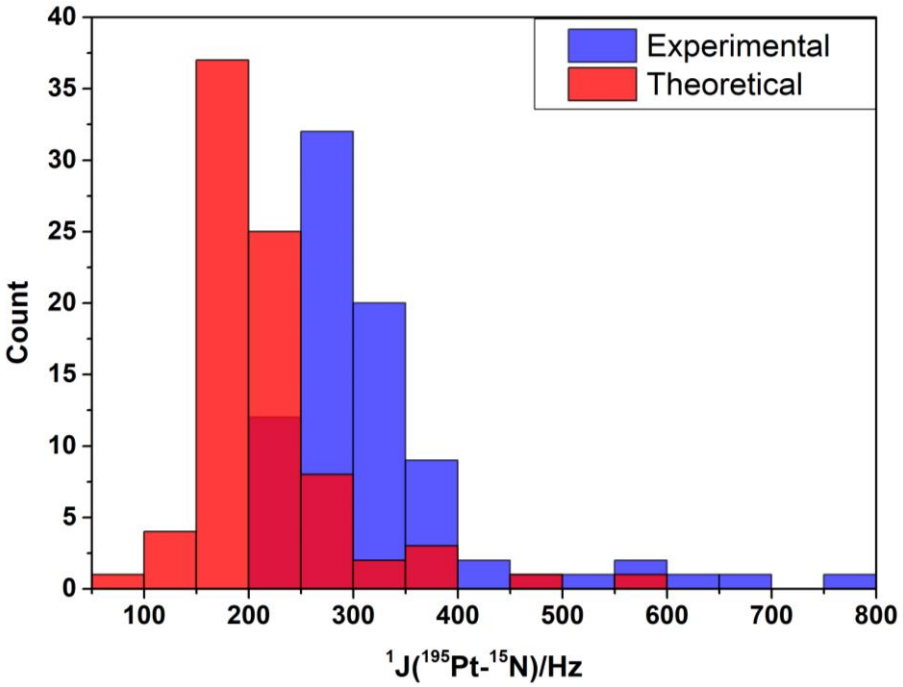

Reference: Own Author.

Figure 4. Calculated and experimental $^{1}J(^{195}Pt\text{-}^{15}N)$, in Hz, for the set of 92 coupling constants in 68 Pt(II) complexes.

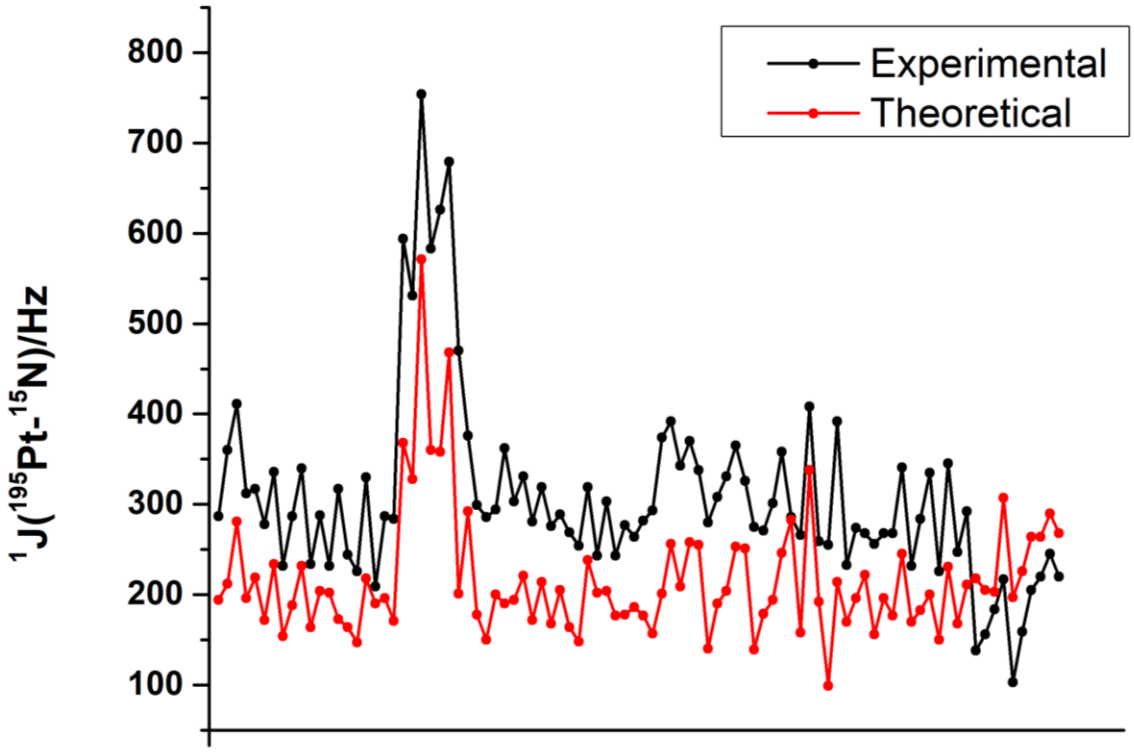

Reference: Own Author.

4.2 STEP 2

The results from the step 2 will be presented.

4.2.1 NMR-DKH basis set modifications

In this section the results obtained from TEST1-5 are presented. These tests consisted in modifications to the NMR-DKH basis set in order to try and improve the coupling constant value obtained using the method in 3.1 (TEST0). Therefore, all results will be compared with TEST0 results. The calculated J-coupling is presented in Table 9 alongside with TEST0 and experimental data.

Table 9. Calculated $^{1}J(^{195}Pt–^{15}N)$ in Hz for the set of 5 coupling constants in 4 Pt(II) complexes in TEST1-5 and at PBEPBE/NMR-DKH/IEFPCM(UFF)//B3LYP/LANL2DZ/def2-SVP/IEFPCM(UFF) (TEST0) level with their respective experimental data

Complex	TEST0	TEST1[a]	TEST2[b]	TEST3[c]	TEST4[d]	TEST5[e]	Expt.
1	212	184	189	189	213	132	360
2	218	188	194	192	245	188	138.3
3	197	170	175	174	224	170	103
4 (*trans* to I^-)	205	176	182	182	235	177	289
4 (*cis* to I^-)	164	144	148	148	178	145	269

[a] Decontraction of all functions and addition of two s functions with high exponent for all atoms, excluding hydrogen, for calculation of J^{FC} contribution; hydrogen atoms had four s functions added; [b] Decontraction of s function for Pt atom; [c] Decontraction of s and p functions for Pt atom; [d] Addition of diffuse functions for all atoms; [e] Same as [a] but with addition of one p function with high exponent for all atoms. Reference: Own Author.

The behavior of J-coupling changes is the same for every complex within the tests: TEST1-3,5 decreased the value of J(Pt-N), whilst TEST4 increased the values. For complexes 1 and 4, underestimated in TEST0, only TEST4 improved the results, since it was the test that caused the J(Pt-N) to increase, although for complex 1 TEST4 provided neglectable improvement of only 1 Hz. For complex 4 J-coupling *trans* to I^- improvement proved more significant, with error going from 29% in TEST0 to 18% in TEST4; for the *cis* J-coupling the error was improved from 39% to 34%. The opposite occurred for complexes 2 and 3, which both presented overestimated coupling constant in TEST0. The given coupling constant was

improved for all tests but TEST4. TEST5 proved, for all four complexes, no or neglectable changes compared to TEST1, showing that addition of p function with high exponent does not improve the calculation of the coupling constant. TEST1 proved better than TEST0, decreasing the error from 58 and 91% to 36 and 65% for complexes 2 and 3 respectively. In general, only TEST1 proved significantly changes in complexes 2 and 3, whilst TESTS2-5 proved no significant change to the calculation.

4.2.2 Functional changes

In this section the results from functional changes are presented. At a total, 10 different functionals were tested in the calculation of J(Pt-N). All functionals tested were hybrid, in contrast to the functional used in TEST0, which is pure (PBEPBE). The functionals used in this section belong to two classes of functionals: GGA and meta-GGA. Also, range-separated functionals were employed. Results from TEST6-15 as well as TEST0 and experimental data are displayed in Table 10.

Table 10. Calculated $^{1}J(^{195}Pt\text{-}^{15}N)$ in Hz for the set of 5 coupling constants in 4 Pt(II) complexes in TEST6-15 and at PBEPBE/NMR-DKH/IEFPCM(UFF)//B3LYP/LANL2DZ/def2-SVP/IEFPCM(UFF) (TEST0) level with their respective experimental data

TEST	Complex 1	Complex 2	Complex 3	Complex 4 (*trans* to I^-)	Complex 4 (*cis* to I^-)
0 (PBEPBE)	212	218	197	205	164
6 (B3LYP)	232	243	220	226	179
7 (TPSSh)	228	234	212	229	172
8 (M06-2X)	255	268	238	242	201
9 (M06)	206	207	193	197	157
10 (CAM-B3LYP)	236	251	224	231	180
11 (LC-ωPBE)	235	237	220	235	177
12 (LC-BLYP)	236	241	222	231	182
13 (BB95)	211	215	194	201	164
14 (mPW1PW91)	236	245	224	236	180
15 (PBE1PBE)	235	245	224	235	178
Expt.	360	138,3	103	289	269

Reference: Own Author.

The first observation to be made is that the use of functional BB95 presented neglectable changes in the coupling constant in comparison with the functional PEBPBE, employed in TEST0. Also, the behavior of changes effectuated by the functionals are the same: they either increased or decreased the coupling constants for the test set. In this matter, only functionals BB95 and M06 decreased the J-coupling, whilst all remaining functionals increased the constant value. Therefore, functionals BB95 and M06 are better for prediction of complexes 2 and 3 that happened to be the ones presenting overestimated coupling constant in TEST0. The functionals B3LYP (TEST6), CAM-B3LYP (TEST10), LC-ωPBE (TEST11), LC-BLYP (TEST12), mPW1PW91 (TEST14) and PBE1PBE (TEST15) all yielded very similar coupling constant values, all increased when compared to TEST0 results. As already said, increasing to the coupling constant improves the results for complexes 1 and 4, the same way that decreasing it improves for complexes 2 and 3. Since all range-separated functionals presented similar results amongst themselves and compared to non-range-separated functionals, it becomes clear that the separation of short and long-range terms does not influence in the calculation of the coupling constant. The functional that, in general, yielded the best results was the M06, decreasing the MDR for the test set from 51.6% to 50.7%.

4.2.3 Basis set variation

In this section, the basis set was varied for both ligand and metal, as well as only for the ligand. This kind of test allows to take conclusions on the efficiency of NMR-DKH on the calculation of coupling constant by comparing its results with results obtained from another basis sets. Also, keeping the basis set for the metal and changing it for the ligands gives an idea of the importance of the basis set for the ligands. For the first part, three basis set were randomly chosen: DZP-DKH, SAPPORO-DZP and SAPPORO-TZP. The two firsts have double-zeta character, whilst the latter has triple-zeta character. All three of them contain relativistic contraction, DKH_2 contraction for the DZP and DKH_3 for the SAPPORO basis set. The relativistic contraction is present only for the metal in the SAPPORO basis sets. For the second part, three functions were randomly chosen for the ligand atoms, keeping the NMR-DKH for the metal: DZP, TZP and cc-pVTZ. The results using these six different basis set are shown in Table 11, alongside with TEST0 and experimental data.

It is evident that results obtained by DZP-DKH and the SAPPORO basis sets presented coupling constants way too unsatisfactory. These results highlight that even though the results from NMR-DKH aren't ideal, yet they're satisfactory when we compare with the ones gotten

from the three basis sets tested. All three basis sets plus the NMR-DKH recover certain relativistic effect due to their relativistic contraction (DKH). The main difference between them lies, perhaps, in the fact that the NMR-DKH basis set was developed for a NMR property calculation.

Table 11. Calculated $^{1}J(^{195}Pt\text{-}^{15}N)$ in Hz for the set of 5 coupling constants in 4 Pt(II) complexes in TEST16-21 and at PBEPBE/NMR-DKH/IEFPCM(UFF)//B3LYP/LANL2DZ/def2-SVP/IEFPCM(UFF) (TEST0) level with their respective experimental data

TEST	Complex 1	Complex 2	Complex 3	Complex 4 (trans to I^-)	Complex 4 (*cis* to I^-)
TEST0	212	218	197	205	164
TEST16[a]	3020	3179	3012	3569	826
TEST17[b]	2473	23127	33059	2320	6953
TEST18[c]	2897	3248	2820	952	415
TEST19[d]	192	196	176	-	-
TEST20[e]	204	210	189	201	159
TEST21[f]	204	208	188	210	157
Expt.	360	138,3	103	289	269

[a] DZP-DKH basis set for both metal and ligand atoms; [b] SAPPORO-DZP-2012 basis set for ligand atoms and SAPPORO-DKH3-DZP-2012 for metal; [c] SAPPORO-TZP-2012 basis set for ligand atoms and SAPPORO-DKH3-DZP-2012 for metal; [d] cc-pVTZ basis set for ligands and NMR-DKH basis set for metal; [e] DZP basis set for ligands and NMR-DKH basis set for metal; [f] TZP basis set for ligands and NMR-DKH basis set for metal. Reference: Own Author.

As for the other three basis set, only for ligand atoms, the results showcase very differently from the ones from TEST16-18. The basis set cc-pVTZ is not described for iodine atom, thus calculation for complex 4 was not run for TEST19. Analyzing the results, it is clear that changing only the basis set for the ligands did not caused much difference for the complex 4. The same occurred for the complexes 1-3 with DZP and TZP basis set. The basis set cc-pVTZ decreased the coupling constant for complexes 1-3, which was good for complexes 2 and 3 that presented overestimated coupling constants. Although the improvement, the decreasing wasn't high enough to yield satisfactory results. With the results, it can be said that changing the basis set only for the ligands isn't a decisive factor in the calculation of the coupling constant J(Pt-N).

4.2.4 Ligand analysis

It becomes clear that the ligands influence on the calculation of the J-coupling property. One interesting factor is that all the overestimated calculated coupling constants J(Pt-N) showcased in section 4.1 present a bulky phosphine or arsine ligand. In order to investigate this relationship better, two tests were made. The first one aimed to analyze the effect of the conformation of the bulky ligands on the calculation of the given property. For this, the complex $[PtCl_2(PBu^n_3)(NH_2(CH_2)_5CH_3)]$ was taken for the test. In TEST22 different conformations of the bulky ligands, hexylamine and tri-butylphosphine, were optimized and then used to calculate the J(Pt-N). In fact, all possible combinations of stable conformations (ANTI and GAUCHE) of the four alkyl groups were taken in the analysis. For the butyl group, the dihedral angle was the only one possible: between carbons one and four of the alkyl group. As for the hexyl group, the dihedral angle taken was the one between carbons two and five, keeping the dihedral angles of C1-C4 and C3-C6 as 180º. At a total 16 different conformations were taken. The coupling constant and all dihedral angles of these 16 conformations as well as the TEST0 and experimental data are displayed in Table 12.

Table 12. Dihedral angles after optimization analyzed on conformational analysis of $[PtCl_2(PBu^n_3)(NH_2(CH_2)_5CH_3)]$ complex with respective calculated $^1J(^{195}Pt\text{-}^{15}N)$, in Hz, at PBEPBE/NMR-DKH/IEFPCM(UFF)//B3LYP/LANL2DZ/def2-SVP/IEFPCM(UFF) level and experimental data

Conformation	α	β	γ	δ	θ	ϕ	J	Expt
I	-179.665	179.538	179.694	179.918	-179.942	-179.946	217	
II	-179.910	65.560	-179.978	-179.975	-179.114	-179.714	218	
III	179.921	-179.587	66.605	179.8	-178.472	-179.506	218	
IV	-179.774	179.725	179.547	-63.408	-175.314	-62.279	217	
V	179.968	64.970	65.372	-179.604	-179.575	-179.903	218	
VI	179.387	65.184	-179.545	-63.190	-176.564	-61.239	218	
VII	-179.447	64.945	179.154	-63.841	-177.531	-61.644	218	138.8
VIII	-179.293	66.409	65.733	-62.931	-176.009	-61.334	219	
IX	64.891	-179.364	-179.943	179.673	-179.833	179.937	218	
X	65.383	65.397	179.322	179.604	-179.357	-179.768	218	
XI	65.769	179.408	66.502	179.678	-179.388	-179.789	218	
XII	65.442	179.255	179.147	-63.494	-175.684	-62.740	217	
XIII	65.706	65.688	65.686	179.623	-178.322	-179.476	218	

(Continued)

Table 12. Continued

Conformation	α	β	γ	δ	θ	ϕ	J	Expt
XIV	65.336	179.217	66.256	-61.978	-174.009	-61.610	218	138.8
XV	65.109	65.041	179.331	-62.513	-174.611	-62.135	218	
XVI	65.772	64.330	64.543	-63.204	-177.222	-61.720	218	
TEST0	-179.337	65.807	-66.986	85.017	-67.317	176.833	218	

Reference: Own Author.

The angles did not vary much from the pre-optimized and post-optimized, with exception of ϕ angle in some conformations. All θ and ϕ angles were kept 180º before. The post-optimized θ angles where all close to 180º in all 16 conformations. The post-optimized ϕ followed the δ angle: if the δ was GAUCHE, so would be the ϕ angle. As for the J-coupling, independently from the conformation the J(Pt-N) didn't vary significantly, ranging from 217 to 219 Hz. The lack of significant variation in the coupling constants indicates that the conformation of bulky ligands doesn't play a key role in the calculation of the given property, even if the ligand itself participates in the coupling mechanism.

The second test regarding the bulky ligands consisted in exchanging the alkyl groups, which causes the bulkiness, for hydrogens, making the ligands non-bulky. For this, four complexes that presented overestimated coupling constants in step 4.1 were randomly chosen. The chosen complexes were: $[PtCl_2(PBu^n_3)(NH_2(CH_2)_5CH_3)]$, $[PtCl_2(AsBu^n_3)(NH_2(CH_2)_5CH_3)]$, $[PtCl_2(PBu^n_3)(aniline)]$ and *cis*-$[Pt(CNS)_2(PEt_3)_2]$. The ligands PBu^n_3 and PEt_3 were substituted by PH_3 and $AsBu^n_3$ was substituted by AsH_3. The geometries were optimized and the coupling constant was calculated according to the computational details in 3.1. The coupling constant obtained in TEST23 as well as TEST0, for comparison, and experimental data are shown in Table 13.

Table 13. Calculated $^1J(^{195}Pt\text{-}^{15}N)$ in Hz for the set of 4 coupling constants in 4 Pt(II) complexes in TEST23 and at PBEPBE/NMR-DKH/IEFPCM(UFF)//B3LYP/LANL2DZ/def2-SVP/IEFPCM(UFF) (TEST0) level with their respective experimental data

Complex	TEST0	TEST23	Expt
$[PtCl_2(PBu^n_3)(NH_2(CH_2)_5CH_3)]$	218	185	138.3
$[PtCl_2(AsBu^n_3)(NH_2(CH_2)_5CH_3)]$	203	178	183.8
$[PtCl_2(PBu^n_3)(aniline)]$	197	159	103
cis-$[Pt(CNS)_2(PEt_3)_2]$	290	323	245

Reference: Own Author.

For the three first complexes in Table 13, the modification of the ligand decreased the coupling constant by 33, 25 and 38 Hz for complexes $[PtCl_2(PBu^n_3)(NH_2(CH_2)_5CH_3)]$, $[PtCl_2(AsBu^n_3)(NH_2(CH_2)_5CH_3)]$, $[PtCl_2(PBu^n_3)(aniline)]$, respectively. Interestingly, the change in the bulky ligand in complex *cis*-$[Pt(CNS)_2(PEt_3)_2]$ did not cause the coupling constant to decrease, on the contrary, the coupling constant in TEST23 is 33 Hz higher than in TEST0. Nevertheless, based on the results in the three first complexes, it is clear that the bulkiness of the ligands plays a key role in the overestimation of the coupling constant. The matter can be evaluated and investigated in further opportunities. For the complex *cis*-$[Pt(CNS)_2(PEt_3)_2]$, the increasing of the coupling constant after changing the bulky phosphine ligand may suggest that the isocyanate ligand may also cause the overestimation of the coupling constant, seeing that all complexes containing isocyanate ligands presented overestimated coupling constant. The isocyanate ligand may also be investigated in further works.

The last analysis in this section is a study of the dependency of the coupling constant with the Pt-N bond length. For this, one complex, cisplatin, was chosen for the study, for being a relatively small complex. This study allows one to conclude whether the geometry optimization is adequate based on the sensibility of the relation bond length-coupling constant. In step 3.1 the cisplatin presented a Pt-N bond length of 2.0938Å and a coupling constant of 195.798 Hz, with an absolute deviation of 116 Hz and relative error of 37% compared to the experimental value. Three different studies were carried out based on the range of the Pt-N bond length variation: 0.001Å, 0.01Å and, also, 0.1Å. These three ranges allow to take conclusions on the behavior of the coupling constant within short and long ranges. Ten times the bond length was varied bellow and above the optimized value of 2.0938Å, totalizing 20 new points for each range and 57 different measures in total. All the 57 coupling constants and the optimized value (marked in the table) is presented in Table 14.

Table 14. Pt-N bond length variation, in Angstrom, and their respective calculated $^1J(^{195}Pt\text{-}^{15}N)$, in Hz, at PBEPBE/NMR-DKH/IEFPCM(UFF)//B3LYP/LANL2DZ/def2-SVP/IEFPCM(UFF) level

Pt-N	J	Pt-N	J	Pt-N	J
1.0938	1163.125	2.0848	197.860	2.1038	193.552
1.1938	523.702	2.0858	197.630	2.1138	191.318
1.2938	69.678	2.0868	197.402	2.1238	189.105
1.3938	206.348	2.0878	197.174	2.1338	186.916
1.4938	300.964	2.0888	196.946	2.1438	184.750

(Continued)

Table 14. Continued

Pt-N	J	Pt-N	J	Pt-N	J
1.5938	317.335	2.0898	196.718	2.1538	182.607
1.6938	301.254	2.0908	196.490	2.1638	180.486
1.7938	274.300	2.0918	196.262	2.1738	178.386
1.8938	246.437	2.0928	196.035	2.1838	176.306
1.9938	219.828	2.0938*	195.798*	2.1938	174.246
2.0038	217.304	2.0948	195.582	2.2938	154.626
2.0138	214.808	2.0958	195.355	2.3938	136.699
2.0238	212.338	2.0968	195.123	2.4938	120.120
2.0338	209.893	2.0978	194.903	2.5938	104.722
2.0438	207.477	2.0988	194.677	2.6938	89.738
2.0538	205.088	2.0998	194.452	2.7938	75.209
2.0638	202.728	2.1008	194.226	2.8938	62.359
2.0738	200.394	2.1018	194.001	2.9938	50.685
2.0838	198.088	2.1028	193.776	3.0938	39.977

* Optimized bond length obtained in TEST0. Reference: Own Author.

To better understand and analyze the behavior of the coupling constant in these studies, three graphics were built for each interval. The first one, Fig. 5, corresponds to the range 0.001.

Figure 5. Calculated $^{1}J(^{195}Pt\text{-}^{15}N)$, in Hz, as function of Pt-N bond length, in Å, for cisplatin ranging from 2.038 to 2.1038Å with a 0.001Å step at PBEPBE/NMRDKH/IEFPCM(UFF)//B3LYP/ LANL2DZ/def2-SVP/IEFPCM(UFF) level

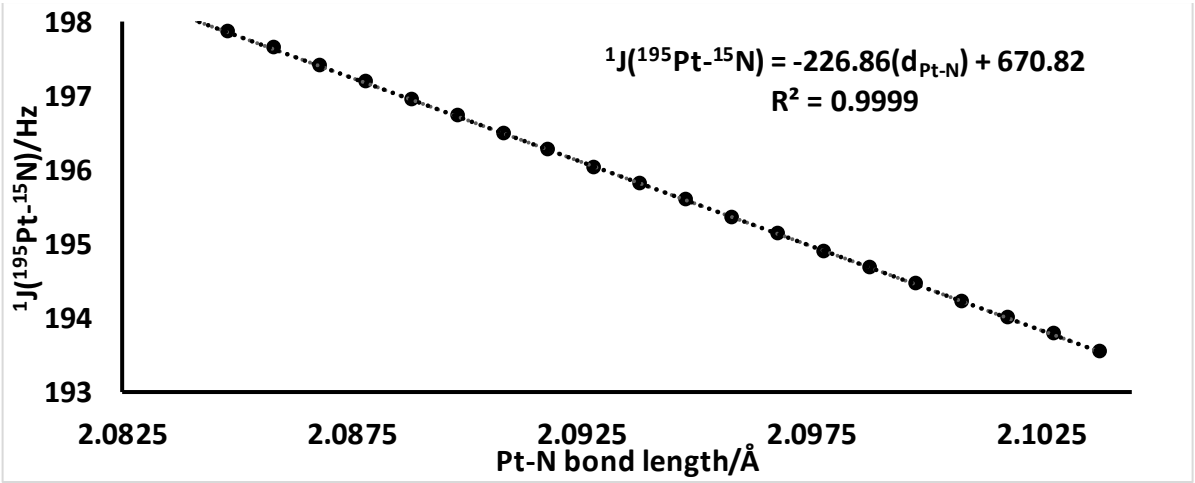

Reference: Own Author.

For the set varying 0.001Å the behavior of the coupling constant is linear with the following relation: $'J\left(^{195}Pt - {}^{15}N\right) = -226.86(d_{Pt-N}) + 670.82$. This relation shows that the coupling constant increases with the decreasing of the bond length. According to this relation, the bond length would have to be 1.5816Å, variating 0.5122Å from the optimized bond length, to yield the experimental value. The experimental Pt-N bond length in Pt(II) complexes ranges from 1.9 to 2.1Å. A Pt-N bond length of 1.5816Å is impractical for Pt(II) complexes.

The results for the studying varying 0.01Å is shown in Figure 6.

Figure 6. Calculated $^{1}J(^{195}Pt\text{-}^{15}N)$, in Hz, as function of Pt-N bond length, in Å, for cisplatin ranging from 1.9938 to 2.1938Å with a 0.01Å step at PBEPBE/NMRDKH/IEFPCM(UFF)//B3LYP/ LANL2DZ/def2-SVP/IEFPCM(UFF) level

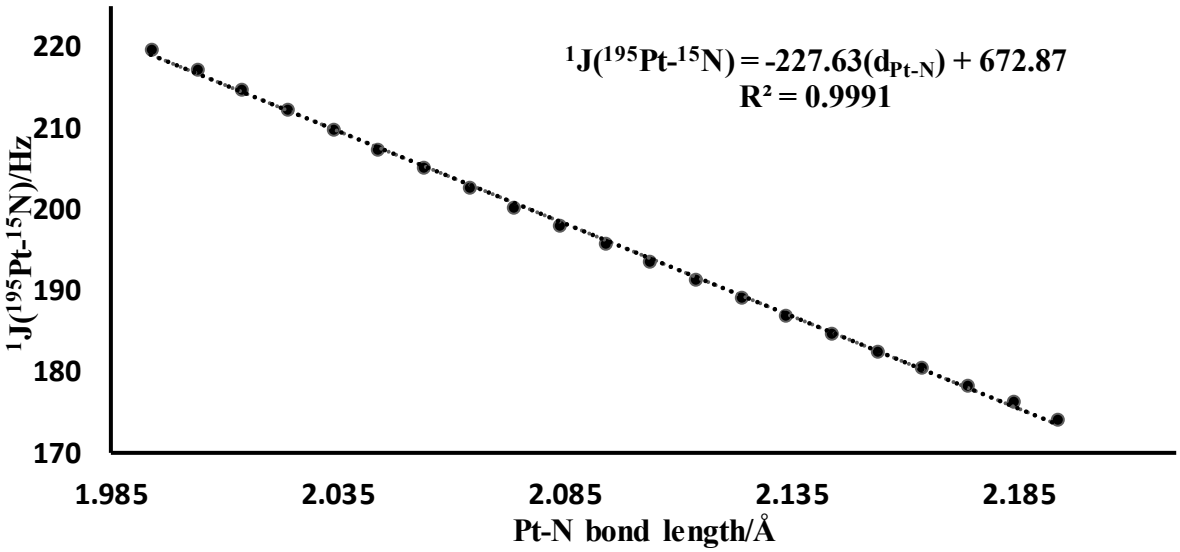

Reference: Own Author.

In this study the relation between J-coupling and the bond length is also linear, although with a determination coefficient of 0.9991, slightly less linear than the previous one. The relation in this study is as following: $'J\left(^{195}Pt - {}^{15}N\right) = -227.63(d_{Pt-N}) + 672.87$, which is very similar to the one above. According to this relation, to yield the experimental value of the coupling constant, the bond length would have to be 1.5853Å, differing from only 0.0037Å in the relation of 0.001Å.

As for the last variation, 0.1Å, the results get very differently from the two above. They are presented in Figure 7. Within this range, it is possible to have a full understanding of the behavior of the coupling constant with the bond length. From the range 1.6 to 2.6Å the dependency on the bond length is linear. From 2.6Å and on the dependency takes an asymptotic

approach. The curious relation comes when the bond length decreases from 1.6Å. At first the coupling decreases until a minimum of 70 Hz when it increases exponentially to a peak of 1163 Hz. The behavior of the J-coupling resembles the Lennard Jones potential curve. No similar study was found on literature that showcases this behavior of J-coupling with the bond length variation. The explanation for this behavior at short bond lengths might come from the overlapping of the orbitals from Pt and N nuclides. Since the J-coupling is a property mediated by the electrons, an overlapping of the orbitals could cause this behavior.

Figure 7. Calculated $^{1}J(^{195}Pt\text{-}^{15}N)$, in Hz, as function of Pt-N bond length, in Å, for cisplatin ranging from 1.0938 to 2.1938Å with a 0.1Å step at PBEPBE/NMRDKH/IEFPCM(UFF)//B3LYP/LANL2DZ/def2-SVP/IEFPCM(UFF) level

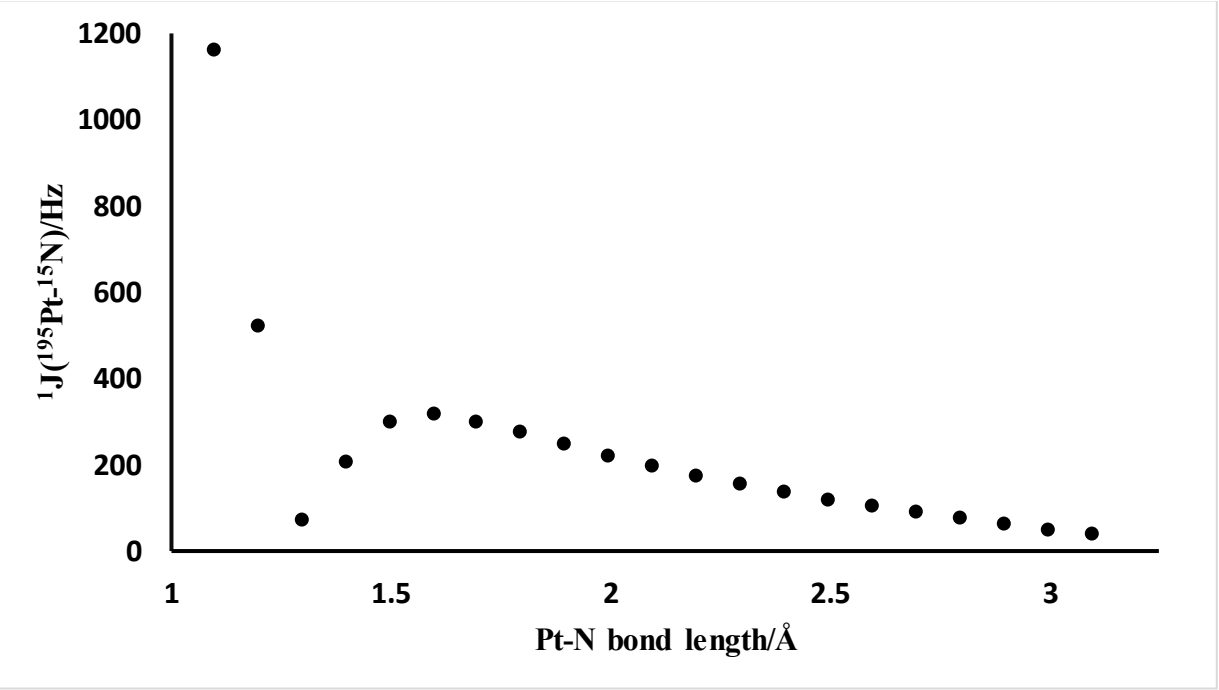

Reference: Own Author.

The most important conclusion from these three studies is that the geometry of the complexes is not a factor for improving the coupling constant, since it would require the bond lengths to be out of the experimental range in order to achieve an accurate coupling constant value.

4.3 STEP 3

In this section, a new protocol was tested for all 67 complexes (92 coupling constants) based on the outcomes from the tests in the previous section. The new protocol was M06/NMR-

DKH(+mixed)/IEFPCM(UFF)//B3LYP/LANL2DZ/def2-SVP/IEFPCM(UFF). The results are shown in Table 15, alongside with the respective experimental data. It is clear that under a general scope the new protocol yielded unsatisfactory results, even compared to the TEST0 protocol. The new MAD was 147 Hz, 37 Hz higher than the MAD of TEST0, and the MRD was 41.3%, 7.3% higher. However, for the ten overestimated complexes this new protocol improved the results over the protocol TEST0. Taking only the overestimated complexes, the MAD was only 20 Hz and the MRD 14.2%. In fact, for the four complexes containing isocyanate complexes the coupling constant was satisfactorily predicted by this new protocol, yielding results with less than 1% of error.

Table 15. Calculated ^{1}J(^{195}Pt–^{15}N) ($^{1}J_{i}^{calc.}$ in Hz) for the set of 92 coupling constants in 67 Pt(II) complexes at M06/NMR-DKH(+mixed)/IEFPCM(UFF)//B3LYP/LANL2DZ/def2SVP/IEFPCM(UFF) level with their respective experimental data

Pt(II) Complexes	Solvent	OBS[a]	$^{1}J_{i}^{calc.}$ [b]	Expt.
[Pt(NH$_3$)$_3$X]				
[Pt(NH$_3$)$_4$]$^{2+}$	H$_2$O		164	287[c]
[Pt(NH$_3$)$_3$(DMSO)]	DMSO	*trans* to NH$_3$	165	288[d]
[Pt(NH$_3$)$_3$(DMSO)]	DMSO	*trans* to DMSO	178	232[d]
[Pt(NH$_3$)$_3$Cl]$^{+}$	DMSO	*trans* to Cl^{-}	184	317[d]
[Pt(NH3)$_3$Cl]$^{+}$	DMSO	*trans* to NH$_3$	145	278[d]
[Pt(NH$_3$)$_3$(H$_2$O)]$^{2+}$	H$_2$O	*trans* to H$_2$O	232	376[e]
[Pt(NH$_3$)$_3$(H$_2$O)]$^{2+}$	H$_2$O	*cis* to H$_2$O	154	299[e]
[Pt(NH$_3$)$_3$(OH)]$^{+}$	H$_2$O	*trans* to OH^{-}	134	286[e]
[Pt(NH$_3$)$_3$(OH)]$^{+}$	H$_2$O	*cis* to OH^{-}	167	294[e]
[Pt(NH$_3$)$_3$(OSO$_3$)]	H$_2$O	*trans* to OSO$_3^{2-}$	165	362[e]
[Pt(NH$_3$)$_3$(OSO$_3$)]	H$_2$O	*cis* to OSO$_3^{2-}$	162	303[e]
[PtCl(NH$_3$)$_3$]$^{+}$	H$_2$O	*trans* to Cl^{-}	186	331[e]
[PtCl(NH$_3$)$_3$]$^{+}$	H$_2$O	*cis* to Cl^{-}	145	281[e]
[PtBr(NH$_3$)$_3$]$^{+}$	H$_2$O	*trans* to Br^{-}	180	319[e]
[PtBr(NH$_3$)$_3$]$^{+}$	H$_2$O	*cis* to Br^{-}	142	276[e]
[PtI(NH$_3$)$_3$]$^{+}$	H$_2$O	*trans* to I^{-}	170	289[e]
[PtI(NH$_3$)$_3$]$^{+}$	H$_2$O	*cis* to I^{-}	138	269[e]
[Pt(NH$_3$)$_3$(NO$_2$)]	H$_2$O	*trans* to NO^{2-}	138	254[e]
[Pt(NH$_3$)$_3$(NO$_2$)]	H$_2$O	*cis* to NO^{2-}	192	319[e]
[Pt(NH$_3$)$_3$(DMSO)]$^{2+}$	H$_2$O	*trans* to DMSO	178	243[e]
[Pt(NH$_3$)$_3$(DMSO)]$^{2+}$	H$_2$O	*cis* to DMSO	165	303[e]
[Pt(NH$_3$)$_3$(tu)]$^{2+}$	H$_2$O	*trans* to tu	156	243[e]

(Continued)

Table 15. Continued

Pt(II) Complexes	Solvent	OBS[a]	$^1J_i^{calc.}$ [b]	Expt.
$[Pt(NH_3)_3(tu)]^{2+}$	H_2O	*cis* to tu	148	277[e]
$[Pt(NH_3)_3(SCN)]^+$	H_2O	*trans* to SCN^-	163	264[e]
$[Pt(NH_3)_3(SCN)]^+$	H_2O	*cis* to SCN^-	147	282[e]
$[Pt(NH_3)_2XY]$				
$[Pt(NH_3)_2(CBDCA)]$	H_2O		178	360[d]
cis-$[Pt(NH_3)_2Cl_2]$	DMSO		163	312[d]
trans-$[Pt(NH_3)_2Cl(DMSO)]^+$	DMSO	*trans* to NH_3	152	287[d]
cis-$[Pt(NH_3)_2Cl(DMSO)]^+$	DMSO	*trans* to Cl^-	186	340[d]
cis-$[Pt(NH_3)_2Cl(DMSO)]^+$	DMSO	*trans* to DMSO	145	234[d]
cis-$[Pt(NH_3)_2(OH)_2]$	H_2O	*trans* to OH^-	138	293[e]
cis-$[Pt(NH_3)_2(H_2O)(OSO_3)]$	H_2O	*trans* to OSO_3^{2-}	172	374[e]
cis-$[Pt(NH_3)_2(H_2O)(OSO_3)]$	H_2O	*trans* to H_2O	206	392[e]
cis-$[PtCl(H_2O)(NH_3)_2]^+$	H_2O	*trans* to Cl^-	177	343[e]
cis-$[PtCl(H_2O)(NH_3)_2]^+$	H_2O	*trans* to H_2O	204	370[e]
cis-$[PtCl(NH_3)_2(OH)]$	H_2O	*trans* to Cl^-	207	338[e]
cis-$[PtCl(NH_3)_2(OH)]$	H_2O	*trans* to OH^-	124	280[e]
cis-$[PtBr_2(NH_3)_2]$	H_2O	*trans* to Br^-	158	308[e]
cis-$[PtBr(H_2O)(NH_3)_2]^+$	H_2O	*trans* to Br^-	172	331[e]
cis-$[PtBr(H_2O)(NH_3)_2]^+$	H_2O	*trans* to H_2O	199	365[e]
cis-$[PtBr(NH_3)_2(OH)]$	H_2O	*trans* to Br^-	204	326[e]
cis-$[PtBr(NH_3)_2(OH)]$	H_2O	*trans* to OH^-	122	275[e]
cis-$[PtI_2(NH_3)_2]$	H_2O	*trans* to I^-	148	271[e]
cis-$[PtI(H_2O)(NH_3)_2]^+$	H_2O	*trans* to I^-	235	301[e]
cis-$[PtI(H_2O)(NH_3)_2]^+$	H_2O	*trans* to H_2O	278	358[e]
cis-$[Pt(NH_3)_2(NO_2)_2]$	H_2O	*trans* to NO^{2-}	157	286[e]
cis-$[Pt(H_2O)(NH_3)_2(NO_2)]^+$	H_2O	*trans* to NO^{2-}	142	266[e]
cis-$[Pt(H_2O)(NH_3)_2(NO_2)]^+$	H_2O	*trans* to H_2O	263	408[e]
cis-$[Pt(NH_3)_2(SCN)_2]$	H_2O	*trans* to SCN^-	161	259[e]
cis-$[Pt(H_2O)(NH_3)_2(DMSO)]^{2+}$	H_2O	*trans* to DMSO	94	255[e]
cis-$[Pt(H_2O)(NH_3)_2(DMSO)]^{2+}$	H_2O	*trans* to H_2O	165	392[e]
cis-$[Pt(NH_3)_2(tu)_2]$	H_2O	*trans* to tu	146	233[e]
cis-$[Pt(NH_3)_2(DMSO)_2]^{2+}$	DMSO	*trans* to DMSO	167	268[f]
cis-$[Pt(NH_3)_2(DMSO)Br]^+$	DMSO	*trans* to Br^-	195	341[f]
cis-$[Pt(NH_3)_2(DMSO)Br]^+$	DMSO	*trans* to DMSO	148	232[f]
trans-$[Pt(NH_3)_2(DMSO)Br]^+$	DMSO	*trans* to NH_3	149	284[f]
$[Pt(NH_3)X_2Y]$				
cis-$[Pt(NH_3)Cl_2(DMSO)]$	DMSO	*trans* to Cl^-	185	336[d]

(Continued)

Table 15. Continued

Pt(II) Complexes	Solvent	OBS[a]	$^1J_i^{calc.}$ [b]	Expt.
trans-[$Pt(NH_3)Cl_2(DMSO)$]	DMSO	*trans* to DMSO	134	232[d]
cis-[$Pt(NH_3)(DMSO)_2(H_2O)]^{2+}$	DMSO	*trans* to DMSO	163	274[f]
cis-[$Pt(NH_3)(DMSO)_2Cl]^{+}$	DMSO	*trans* to DMSO	152	268[f]
trans-[$Pt(NH_3)(DMSO)(H_2O)_2]^{2+}$	DMSO	*trans* to DMSO	135	256[f]
cis-[$Pt(NH_3)(DMSO)_2Br]^{+}$	DMSO	*trans* to DMSO	149	268[f]
cis-[$Pt(NH_3)(DMSO)Br_2$]	DMSO	*trans* to Br^-	161	335[f]
trans-[$Pt(NH_3)(DMSO)Br_2$]	DMSO	*trans* to DMSO	129	226[f]
[$Pt(NO_2)_3X$]				
$[Pt(NO_2)_4]^{2-}$	H_2O	*trans* to NO^{2-}	286	594[g]
$[Pt(H_2O)(NO_2)_3]^-$	H_2O	*trans* to NO^{2-}	263	531[g]
$[Pt(H_2O)(NO_2)_3]^-$	H_2O	*trans* to H_2O	416	754[g]
$[Pt(NO_2)_3(OH)]^{2-}$	H_2O	*trans* to NO^{2-}	285	583[g]
$[Pt(NO_2)_3(OH)]^{2-}$	H_2O	*trans* to H_2O	270	626[g]
[$Pt(NO_2)_2X_2$]				
cis-[$Pt(H_2O)_2(NO_2)_2$]	H_2O	*trans* to H_2O	353	679[g]
trans-[$Pt(H_2O)_2(NO_2)_2$]	H_2O	*trans* to NO^{2-}	165	470[g]
[$Pt(NCS)_2X_2$]				
cis-[$Pt(CNS)_2(PMe_2Et)_2$]	$(CD_3)_2SO$	Isomer NS	217	205[h]
cis-[$Pt(CNS)_2(PMe_2Et)_2$]	$(CD_3)_2SO$	Isomer NN	218	220[h]
cis-[$Pt(CNS)_2(PEt_3)_2$]	CH_2Cl_2	Isomer NS	233	245[h]
cis-[$Pt(CNS)_2(PEt3)_2$]	CH_2Cl_2	Isomer NN	221	220[h]
[Pt(N-hexyl)X_2Y]				
[$PtCl_2(AsMePh_2)(NH_2(CH_2)_5CH_3)$]	$CDCl_3$		158	209[i]
[$PtCl_2(NH_2(CH_2)_5CH_3)_2$]	$CDCl_3$		164	287[i]
[$PtCl_2(C_2H_4)(NH_2(CH_2)_5CH_3)$]	$CDCl_3$		145	284[i]
[$PtCl_2(PBu^n_3)(NH_2(CH_2)_5CH_3)$]	$CDCl_3$		176	138.3[i]
[$PtCl_2(PMePh_2)(NH_2(CH_2)_5CH_3)$]	$CDCl_3$		168	155.9[i]
[$PtCl_2(AsBu^n_3)(NH_2(CH_2)_5CH_3)$]	$CDCl_3$		166	183.8[i]
Unsorted				
$[Pt(en)(H_2O)_2]^{2+}$	H_2O		228	411[d]
cis-[$PtCl_2(Gly)]^-$	DMSO	*trans* to Cl^-	149	317[d]
trans-[$PtCl_2(Gly)(DMSO)$]	DMSO	*trans* to DMSO	143	244[d]
[Pt(Cl(Gly)(DMSO)] (O-gly *trans* to Cl)	DMSO	*trans* to DMSO	135	226[d]
[PtCl(Gly)(DMSO)] (N-gly *trans* to Cl)	DMSO	*trans* to Cl^-	180	330[d]
$[Pt(en)(DMSO)I]^+$	DMSO	*trans* to I^-	183	345[f]
$[Pt(en)(DMSO)I]^+$	DMSO	*trans* to DMSO	147	247[f]
$[Pt(en)(DMSO)_2]^{2+}$	DMSO	*trans* to DMSO	179	292[f]

(Continued)

Table 15. Continued

Pt(II) Complexes	Solvent	OBS[a]	$^1J_i^{calc.}$ [b]	Expt.
$[PtCl_2(PBu^n_3)(t\text{-}Bu(N{=}CH_2)]$	CD_2Cl_2		240	217[j]
$[PtCl_2(PBu^n_3)(aniline)]$	$CDCl_3$		165	103[j]
$[PtCl_2(PBu^n_3)(t\text{-butylamine})$	$CDCl_3$		182	159[j]
		MAD	**147 Hz**	
		MRD	**41.3%**	

[a] Observation: position of ^{15}N atom coupling with ^{195}Pt; [b] Calculated values at PBEPBE/NMR-DKH/IEFPCM(UFF)//B3LYP/LANL2DZ/def2-SVP/IEFPCM(UFF) protocol; [c] LEVASON, *et al*, 1993; [d] STILL, *et al*, 2007; [e] APPELTON, *et al*, 1986; [f] KERRISON, *et al*, 1985; [g] WOOD, *et al*, 1983; [h] ANDERSON, *et al*, 1976; [i] MOTSCHI, *et al*, 1979; [j] POEL, *et al*, 1981. Reference: Own Author.

Since the overestimated complexes are such minority in face of the full set of complexes (10 in 92 coupling constants), this protocol cannot be taken as the appropriated one for the calculation of the $^1J(^{195}Pt\text{-}^{15}N)$ coupling constant.

4.4 STEP 4

Since coming up with an appropriated protocol for both under and overestimated complexes was not possible, in this section, all the 10 complexes that presented overestimated constant with TEST0 protocol were left aside and the remaining 57, or 82 coupling constants, were taken in order to try and improve the outcomes. As already pointed out in section 4.1, even though underestimated, the profile of the calculated coupling constants is very similar to the experimental ones (Fig. 4). This similarity shows that even though the methodology applied underestimates the coupling constant, the error within the values are systematical and can be corrected by a scaling procedure. The two scaling procedures are detailed in section 3.4.

(a) Mean Relative Error (model 1)

Using experimental and calculated values of the underestimated coupling constants from Table 8 in Eq. (4) we found $\bar{E}\%$=33.8% giving S=1.51 according to Eq. (3). So, the scaling Model 1 is represented as in Equation (7).

$$^1J_i^{scal.-1} = 1.51\ ^1J_i^{calc.} \quad (7)$$

Since the coupling constants calculated were all underestimated, the scaling factor must be higher than unity in order to approximate the calculated to the experimental data. To apply this method, though, it is important that all calculated data behaves in the same way, otherwise, the method would not work, since it would either deviate the under or overestimated values further from the experimental data (hence leaving aside the overestimated constants).

(b) Least Squares Method (model 2)

This method intended to find a correlation between the calculated and experimental coupling constants. For this, the underestimated data was plotted against the experimental data, as shown in Figure 8, and a linear relation was discovered by means of the least squares method.

Figure 8. Linear regression between the underestimated calculated and experimental $^{1}J(^{195}Pt\text{-}^{15}N)$ for the set of 82 coupling constants used to obtain the Model 2.

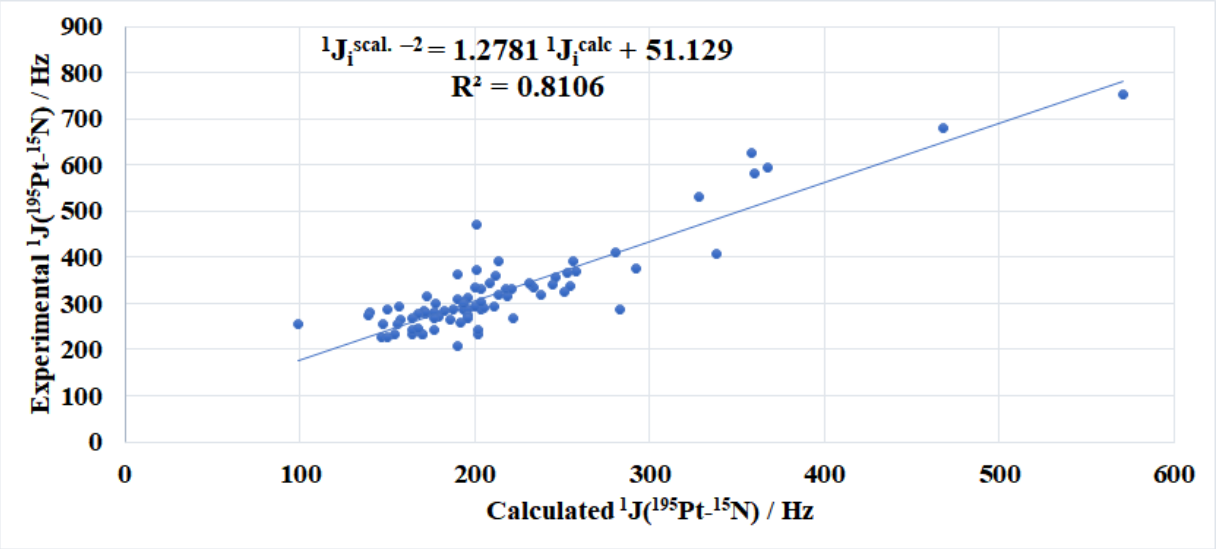

Reference: Own Author.

The linear correlation Model 2 is represented by Equation (8) with a determination coefficient R^2=0.8106, as shown in Fig. 7.

$$^{1}J_i^{scal.-2} = 1.2781\ ^{1}J_i^{calc.} + 51.129 \quad (8)$$

All scaled values by both scaling models are shown in Table 16, alongside with experimental data and TEST0 for comparison purposes. Both models proved to improve

significantly the calculated coupling constants. The scaled coupling constants by Model 1 presented MRD and MAD of 10.3% and 33 Hz, respectively, much lower than those found for original calculated data (33.8% and 111 Hz). If we take the $^{1}J(^{195}Pt–^{15}N)$ coupling constant spectral window as 600 Hz (ranging from 100 to 700 Hz), 33 Hz represents only 5.5% of the spectral window, a very satisfactory result. Analyzing the results from the linear correlation Model 2, the mean relative error and the absolute deviation are 9.8% and 31 Hz, respectively, slightly better than Model 1. The MAD for Model 2 represents 5.2% of the spectral window of the $^{1}J(^{195}Pt–^{15}N)$ coupling constants. Both models prove to be satisfactory when predicting $^{1}J(^{195}Pt–^{15}N)$ coupling constant. Fig. 9 also presents a comparison between the calculated values and those corrected with the scaling factors. An important achievement was that both models were capable of distinguishing the coupling constant in *cis* and *trans* isomers ([Pt(NH$_3$)Cl$_2$(DMSO)], [Pt(NH$_3$)$_2$Cl(DMSO)]$^+$, [Pt(H$_2$O)$_2$(NO$_2$)$_2$] and [Pt(NH$_3$)(DMSO)Br$_2$]), which can be very helpful for experimentalists.

Table 16. Scaled $^{1}J(^{195}Pt–^{15}N)$ by Model 1 ($^{1}J_i^{scal.-1}$) and Model 2 ($^{1}J_i^{scal.-2}$), in Hz, for the set of 82 coupling constants in 57 Pt(II) complexes, experimental values and calculated coupling constant ($^{1}J_i^{calc}$), in Hz, at PBEPBE/NMR-DKH/IEFPCM(UFF)//B3LYP/LANL2DZ/def2SVP/IEFPCM(UFF) level.

Pt(II) Complexes	Solvent	OBS[a]	$^{1}J_i^{calc.}$ [b]	$^{1}J_i^{scal.-1}$ [c]	$^{1}J_i^{scal.-2}$ [d]	Expt.
[Pt(NH$_3$)$_3$X]						
[Pt(NH$_3$)$_4$]$^{2+}$	H$_2$O		194	293	299	287[e]
[Pt(NH$_3$)$_3$(DMSO)]	DMSO	*trans* to NH$_3$	204	308	312	288[f]
[Pt(NH$_3$)$_3$(DMSO)]	DMSO	*trans* to DMSO	202	305	310	232[f]
[Pt(NH$_3$)$_3$Cl]$^+$	DMSO	*trans* to Cl$^-$	219	331	331	317[f]
[Pt(NH3)$_3$Cl]$^+$	DMSO	*trans* to NH$_3$	172	260	271	278[f]
[Pt(NH$_3$)$_3$(H$_2$O)]$^{2+}$	H$_2$O	*trans* to H$_2$O	292	441	425	376[g]
[Pt(NH$_3$)$_3$(H$_2$O)]$^{2+}$	H$_2$O	*cis* to H$_2$O	178	269	279	299[g]
[Pt(NH$_3$)$_3$(OH)]$^+$	H$_2$O	*trans* to OH$^-$	150	227	243	286[g]
[Pt(NH$_3$)$_3$(OH)]$^+$	H$_2$O	*cis* to OH$^-$	200	302	307	294[g]
[Pt(NH$_3$)$_3$(OSO$_3$)]	H$_2$O	*trans* to OSO$_3^{2-}$	190	287	294	362[g]
[Pt(NH$_3$)$_3$(OSO$_3$)]	H$_2$O	*cis* to OSO$_3^{2-}$	194	293	299	303[g]
[PtCl(NH$_3$)$_3$]$^+$	H$_2$O	*trans* to Cl$^-$	221	334	334	331[g]
[PtCl(NH$_3$)$_3$]$^+$	H$_2$O	*cis* to Cl$^-$	172	260	271	281[g]
[PtBr(NH$_3$)$_3$]$^+$	H$_2$O	*trans* to Br$^-$	214	323	325	319[g]
[PtBr(NH$_3$)$_3$]$^+$	H$_2$O	*cis* to Br$^-$	168	254	266	276[g]
[PtI(NH$_3$)$_3$]$^+$	H$_2$O	*trans* to I$^-$	205	310	314	289[g]

(Continued)

Table 16. Continued

Pt(II) Complexes	Solvent	OBS[a]	${}^1J_i^{calc.}$ [b]	${}^1J_i^{scal.-1}$ [c]	${}^1J_i^{scal.-2}$ [d]	Expt.
$[PtI(NH_3)_3]^+$	H_2O	*cis* to I^-	164	248	261	269[g]
$[Pt(NH_3)_3(NO_2)]$	H_2O	*trans* to NO^{2-}	148	223	241	254[g]
$[Pt(NH_3)_3(NO_2)]$	H_2O	*cis* to NO^{2-}	238	359	356	319[g]
$[Pt(NH_3)_3(DMSO)]^{2+}$	H_2O	*trans* to DMSO	202	305	310	243[g]
$[Pt(NH_3)_3(DMSO)]^{2+}$	H_2O	*cis* to DMSO	204	308	312	303[g]
$[Pt(NH_3)_3(tu)]^{2+}$	H_2O	*trans* to tu	177	267	278	243[g]
$[Pt(NH_3)_3(tu)]^{2+}$	H_2O	*cis* to tu	178	269	279	277[g]
$[Pt(NH_3)_3(SCN)]^+$	H_2O	*trans* to SCN^-	186	281	289	264[g]
$[Pt(NH_3)_3(SCN)]^+$	H_2O	*cis* to SCN^-	177	267	278	282[g]
$[Pt(NH_3)_2XY]$						
$[Pt(NH_3)_2(CBDCA)]$	H_2O		212	320	322	360[f]
cis-$[Pt(NH_3)_2Cl_2]$	DMSO		196	296	302	312[f]
trans-$[Pt(NH_3)_2Cl(DMSO)]^+$	DMSO	*trans* to NH_3	188	284	292	287[f]
cis-$[Pt(NH_3)_2Cl(DMSO)]^+$	DMSO	*trans* to Cl^-	232	350	348	340[f]
cis-$[Pt(NH_3)_2Cl(DMSO)]^+$	DMSO	*trans* to DMSO	164	248	261	234[f]
cis-$[Pt(NH_3)_2(OH)_2]$	H_2O	*trans* to OH^-	157	237	252	293[g]
cis-$[Pt(NH_3)_2(H_2O)(OSO_3)]$	H_2O	*trans* to OSO_3^{2-}	201	304	308	374[g]
cis-$[Pt(NH_3)_2(H_2O)(OSO_3)]$	H_2O	*trans* to H_2O	256	387	379	392[g]
cis-$[PtCl(H_2O)(NH_3)_2]^+$	H_2O	*trans* to Cl^-	209	316	319	343[g]
cis-$[PtCl(H_2O)(NH_3)_2]^+$	H_2O	*trans* to H_2O	258	390	381	370[g]
cis-$[PtCl(NH_3)_2(OH)]$	H_2O	*trans* to Cl^-	255	385	378	338[g]
cis-$[PtCl(NH_3)_2(OH)]$	H_2O	*trans* to OH^-	140	211	230	280[g]
cis-$[PtBr_2(NH_3)_2]$	H_2O	*trans* to Br^-	190	287	294	308[g]
cis-$[PtBr(H_2O)(NH_3)_2]^+$	H_2O	*trans* to Br^-	204	308	312	331[g]
cis-$[PtBr(H_2O)(NH_3)_2]^+$	H_2O	*trans* to H_2O	253	382	375	365[g]
cis-$[PtBr(NH_3)_2(OH)]$	H_2O	*trans* to Br^-	251	379	372	326[g]
cis-$[PtBr(NH_3)_2(OH)]$	H_2O	*trans* to OH^-	139	210	229	275[g]
cis-$[PtI_2(NH_3)_2]$	H_2O	*trans* to I^-	179	270	280	271[g]
cis-$[PtI(H_2O)(NH_3)_2]^+$	H_2O	*trans* to I^-	194	293	299	301[g]
cis-$[PtI(H_2O)(NH_3)_2]^+$	H_2O	*trans* to H_2O	246	371	366	358[g]
cis-$[Pt(NH_3)_2(NO_2)_2]$	H_2O	*trans* to NO^{2-}	283	427	413	286[g]
cis-$[Pt(H_2O)(NH_3)_2(NO_2)]^+$	H_2O	*trans* to NO^{2-}	158	239	253	266[g]
cis-$[Pt(H_2O)(NH_3)_2(NO_2)]^+$	H_2O	*trans* to H_2O	338	510	484	408[g]
cis-$[Pt(NH_3)_2(SCN)_2]$	H_2O	*trans* to SCN^-	192	290	297	259[g]
cis-$[Pt(H_2O)(NH_3)_2(DMSO)]^{2+}$	H_2O	*trans* to DMSO	99	149	178	255[g]
cis-$[Pt(H_2O)(NH_3)_2(DMSO)]^{2+}$	H_2O	*trans* to H_2O	214	323	325	392[g]
cis-$[Pt(NH_3)_2(tu)_2]$	H_2O	*trans* to tu	170	257	269	233[g]

(Continued)

Table 16. Continued

Pt(II) Complexes	Solvent	OBS[a]	$^1J_i^{calc.}$ [b]	$^1J_i^{scal.-1}$ [c]	$^1J_i^{scal.-2}$ [d]	Expt.
cis-$[Pt(NH_3)_2(DMSO)_2]^{2+}$	DMSO	*trans* to DMSO	196	296	302	268[h]
cis-$[Pt(NH_3)_2(DMSO)Br]^{+}$	DMSO	*trans* to Br^-	245	370	365	341[h]
cis-$[Pt(NH_3)_2(DMSO)Br]^{+}$	DMSO	*trans* to DMSO	170	257	269	232[h]
trans-$[Pt(NH_3)_2(DMSO)Br]^{+}$	DMSO	*trans* to NH_3	183	248	261	284[h]
$[Pt(NH_3)X_2Y]$						
cis-$[Pt(NH_3)Cl_2(DMSO)]$	DMSO	*trans* to Cl^-	234	353	351	336[f]
trans-$[Pt(NH_3)Cl_2(DMSO)]$	DMSO	*trans* to DMSO	154	233	248	232[f]
cis-$[Pt(NH_3)(DMSO)_2(H_2O)]^{2+}$	DMSO	*trans* to DMSO	196	296	302	274[h]
cis-$[Pt(NH_3)(DMSO)_2Cl]^{+}$	DMSO	*trans* to DMSO	222	335	335	268[h]
trans-$[Pt(NH_3)(DMSO)(H_2O)_2]^{2+}$	DMSO	*trans* to DMSO	156	236	251	256[h]
cis-$[Pt(NH_3)(DMSO)_2Br]^{+}$	DMSO	*trans* to DMSO	177	267	278	268[h]
cis-$[Pt(NH_3)(DMSO)Br_2]$	DMSO	*trans* to Br^-	200	335	302	335[h]
trans-$[Pt(NH_3)(DMSO)Br_2]$	DMSO	*trans* to DMSO	150	226	227	226[h]
$[Pt(NO_2)_3X]$						
$[Pt(NO_2)_4]^{2-}$	H_2O	*trans* to NO^{2-}	368	556	522	594[i]
$[Pt(H_2O)(NO_2)_3]^-$	H_2O	*trans* to NO^{2-}	328	495	471	531[i]
$[Pt(H_2O)(NO_2)_3]^-$	H_2O	*trans* to H_2O	571	862	782	754[i]
$[Pt(NO_2)_3(OH)]^{2-}$	H_2O	*trans* to NO^{2-}	360	544	512	583[i]
$[Pt(NO_2)_3(OH)]^{2-}$	H_2O	*trans* to H_2O	358	541	509	626[i]
$[Pt(NO_2)_2X_2]$						
cis-$[Pt(H_2O)_2(NO_2)_2]$	H_2O	*trans* to H_2O	468	707	650	679[i]
trans-$[Pt(H_2O)_2(NO_2)_2]$	H_2O	*trans* to NO^{2-}	201	304	308	470[i]
$[Pt(N\text{-}hexyl)X_2Y]$						
$[PtCl_2(AsMePh_2)(NH_2(CH_2)_5CH_3)]$	$CDCl_3$		190	287	294	209[j]
$[PtCl_2(NH_2(CH_2)_5CH_3)_2]$	$CDCl_3$		196	296	302	287[j]
$[PtCl_2(C_2H_4)(NH_2(CH_2)_5CH_3)]$	$CDCl_3$		171	258	270	284[j]
Unsorted						
$[Pt(en)(H_2O)_2]^{2+}$	H_2O		281	424	411	411[f]
cis-$[PtCl_2(Gly)]^-$	DMSO	*trans* to Cl^-	173	261	273	317[f]
trans-$[PtCl_2(Gly)(DMSO)]$	DMSO	*trans* to DMSO	164	248	261	244[f]
[Pt(Cl(Gly)(DMSO)] (O-gly *trans* to Cl)	DMSO	*trans* to DMSO	147	222	239	226[f]
[PtCl(Gly)(DMSO)] (N-gly *trans* to Cl)	DMSO	*trans* to Cl^-	218	329	330	330[f]
$[Pt(en)(DMSO)I]^+$	DMSO	*trans* to I^-	231	345	349	345[h]

(Continued)

Table 16. Continued

Pt(II) Complexes	Solvent	OBS[a]	$^1J_i^{calc.}$ [b]	$^1J_i^{scal.-1}$ [c]	$^1J_i^{scal.-2}$ [d]	Expt.
$[Pt(en)(DMSO)I]^+$	DMSO	*trans* to DMSO	168	247	254	247[h]
$[Pt(en)(DMSO)_2]^{2+}$	DMSO	*trans* to DMSO	211	292	319	292[h]
		MAD	**111 Hz**	**33 Hz**	**31 Hz**	
		MRD	**33.8%**	**10.3%**	**9.8%**	

[a] Observation: position of ^{15}N atom coupling with ^{195}Pt. [b] Calculated values at PBEPBE/NMR-DKH/IEFPCM(UFF)//B3LYP/LANL2DZ/def2-SVP/IEFPCM(UFF) protocol. [c] Scaled values according to Model 1: $^1J_i^{scal.-1} = 1.51\ ^1J_i^{calc.}$. [d] Scaled values according to Model 2: $^1J_i^{scal.-2} = 1.278\ ^1J_i^{calc.} + 51.129$. [e] LEVASON, *et al*, 1993; [f] STILL, *et al*, 2007; [g] MOTSCHI, *et al*, 1979; [h] WOOD, *et al*, 1983; [i] APPELTON, *et al*, 1986; [j] KERRISON, *et al*, 1985. Reference: Own Author.

In order to validate the scaling procedures, a set of 14 complexes, not belonging to the original set, were taken to test the availability of Models 1 and 2. At a total, 16 different $^1J(^{195}Pt–^{15}N)$ coupling constants were tested. The very same methodology was applied to calculate the $^1J(^{195}Pt–^{15}N)$ coupling constant for this set of 14 complexes, namely, PBEPBE/NMR-DKH/IEFPCM(UFF)//B3LYP/ LANL2DZ/def2-SVP/IEFPCM(UFF). The calculated and scaled values from the validation set are displayed in Table 17. All calculated values presented in Table 17 have underestimated values compared with respective experimental data, which is important since both models are based on an underestimated set of data. The mean relative error and absolute deviation of the calculated coupling constants are 36.7% and 164 Hz, respectively. It is noticeable that the mean relative error is similar to the first set of data, whereas the absolute deviation is higher due to complexes with high coupling constants in the validation set.

Table 17. Experimental, calculated and scaled $^1J(^{195}Pt-^{15}N)$ coupling constants, in Hz, for the validation set of data.

Pt(II) Complexes	OBS[a]	$^1J_i^{calc.}$ [b]	$^1J_i^{scal.-1}$ [c]	$^1J_i^{scal.-2}$ [d]	Expt.
trans-$[PtCl_2(py)_2]$		197	298	304	400[e]
$[Pt(oeimp)(PBu^n_3)]$		214	323	325	294.1[f]
$[Pt(oeimp)(P(OEt)_3)]$		230	347	345	303[f]
$[Pt(oeimp)(AsBu^n_3)]$		250	378	372	366.2[f]
[Pt(oeimp)(pip)]		309	467	447	464.7[f]
$[Pt(oeimp)(NH_2(CH_2)_5CH_3)]$	*trans* to $NH_2(CH_2)_5CH_3$	314	475	454	478[f]

(Continued)

Table 17. Continued

Pt(II) Complexes	OBS[a]	$^1J_i^{calc.}$ [b]	$^1J_i^{scal.-1}$ [c]	$^1J_i^{scal.-2}$ [d]	Expt.
[Pt(oeimp)($NH_2(CH_2)_5CH_3$)]	*trans* to N-oeimp	190	286	294	316[f]
[Pt(oeimp)(py)]		310	469	448	494.2[f]
trans-[$Pt(SCN)_2(NMe_3)_2$]	Isomer NN	440	665	615	504[g]
trans-[$Pt(NH_3)_2Cl_2$]		159	240	254	280[h]
cis-[$Pt(NH_3)_2$(4-mepy)Cl]$^{+1}$		158	239	254	276[i]
trans-[$Pt(NO_2)_2Br_2]^{2-}$		173	262	273	452[j]
cis-[$Pt(NO_2)_2ClBr]^{2-}$	*trans* to Cl^-	388	585	547	665[j]
cis-[$Pt(NO_2)_2ClBr]^{2-}$	*trans* to Br^-	431	650	602	665[j]
$[Pt(NO_2)_3Cl]^{2-}$	*trans* to Cl^-	594	897	812	757[j]
$[Pt(NO_2)_3Cl]^{2-}$	*trans* to Br^-	266	402	392	535[j]
	MAD	**164 Hz**	**65 Hz**	**63 Hz**	
	MRD	**36.7%**	**14.3%**	**13.5%**	

[a] Observation: position of ^{15}N atom coupling with ^{195}Pt; [b] Calculated values at PBEPBE/NMR-DKH/IEFPCM(UFF)//B3LYP/LANL2DZ/def2-SVP/IEFPCM(UFF) protocol; [c] Scaled values according to Model 1: $^1J_i^{scal.-1} = 1.51\ ^1J_i^{calc.}$; [d] Scaled values according to Model 2: $^1J_i^{scal.-2} = 1.278\ ^1J_i^{calc.} + 51.129$; [e] SUTTER, *et al*, 2012; [f] MOTSCHI, *et al*, 1980; [g] ANDERSON, *et al*, 1976; [h] ARVANITIS, 1997; [i] JIN, 2005; [j] KERRISON, 1982. Reference: Own Author.

Figure 9. Calculated, scaled and experimental $^1J(^{195}Pt–^{15}N)$, in Hz, for the set of 82 coupling constants in 57 Pt(II) complexes

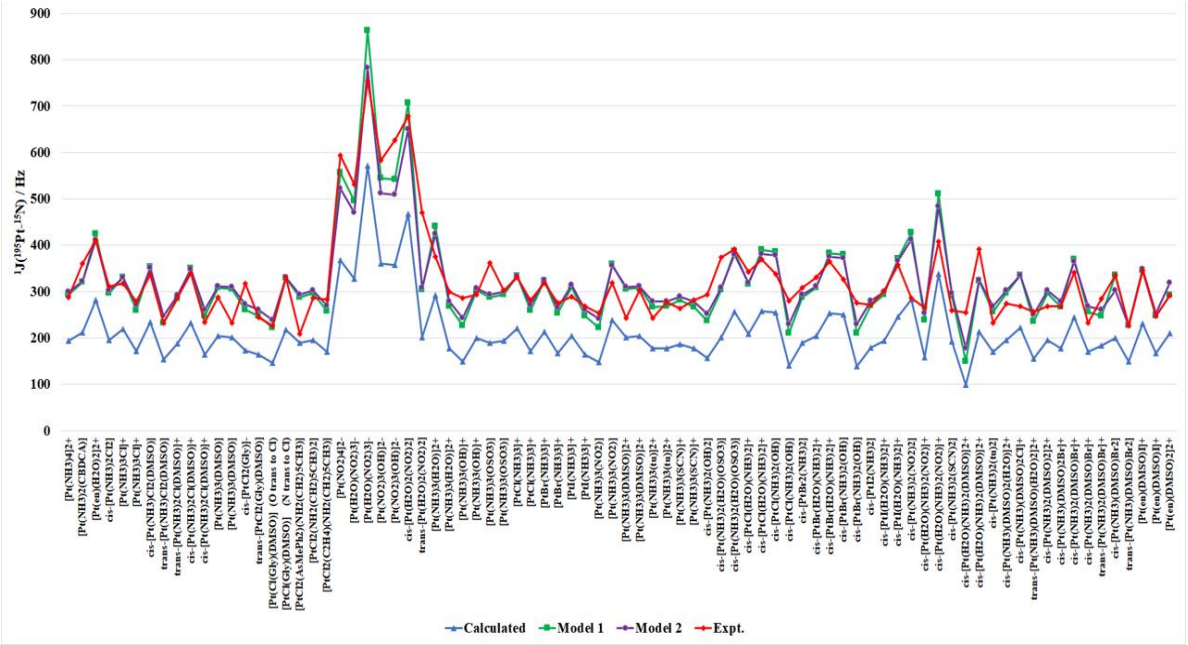

Reference: Own Author.

Taking the scaled coupling constants, both methods showed improved results, increasing the value of the coupling constant, as can be seen in Fig. 10. When scaled by Model 1, the validation set presented mean relative error and absolute deviation of 14.3% and 65 Hz, respectively. As for the scaling Model 2, the validation set presented a mean relative error and absolute deviation of 13.5% and 63 Hz. Although presenting higher mean deviation, the results obtained by both models were very satisfactory, being the Model 2 slightly better than the Model 1. We can also compare the results obtained in this work with those from Sutter and coworkers (SUTTER, *et al*, 2011), since all four complexes (*cis*-[$Pt(NH_3)_2Cl_2$]; *cis*-[$Pt(NH_3)_2Br_2$]; *cis*-[$Pt(NH_3)_2(OH)_2$]; *cis*-[$Pt(NH_3)_2(OH)Cl$]) studied in their work are present in our data set. It is important to highlight that for the *cis*-[$Pt(NH_3)_2Cl_2$] complex the solvents differ, being DMSO in this work and water in Sutter and coworkers' paper. Since experimental data reported in this work and by Sutter are different, an appropriate measure to compare both results is the MRD, where the MRD for the set of four complexes were 10.6% for Sutter and 10.2% in this work. These results showed that both scaling Models can satisfactorily predict the $^1J(^{195}Pt–^{15}N)$ in Pt(II) complexes. Since the coupling constant is a very sensitive and difficult property to predict, achieving a value that differs of approximately 14% from the experimental data using affordable quantum mechanics level of theory is, indeed, a solid achievement.

Finally, the scaling models proposed here for calculating the $^1J(^{195}Pt–^{15}N)$ coupling constant in Pt(II) complexes can be joined to that from our previous study on the ^{195}Pt chemical shift prediction (PASCHOAL, *et al*, 2016). From a single job run at PBEPBE/NMR-DKH/IEFPCM(UFF) level, using our own NMR-DKH basis set for all atoms, the shielding constant σ for Pt nucleus and $^1J_i^{calc.}$ ($^1J(^{195}Pt–^{15}N)$) coupling constant are calculated. The scaled improved values are them obtained from Equations (8) and (9) (PASCHOAL, *et al*, 2016).

$$\delta = 10.9250\sigma - 2065.7558 \quad (9)$$

With this protocol the expected MAD is 98 Hz (10.4%) and 168 ppm (5%) for coupling constant and chemical shift, respectively.

Figure 10. Calculated $^{1}J(^{195}Pt\text{-}^{15}N)$, in Hz, for the set of 16 coupling constants in 14 Pt(II) complexes used to validate the models.

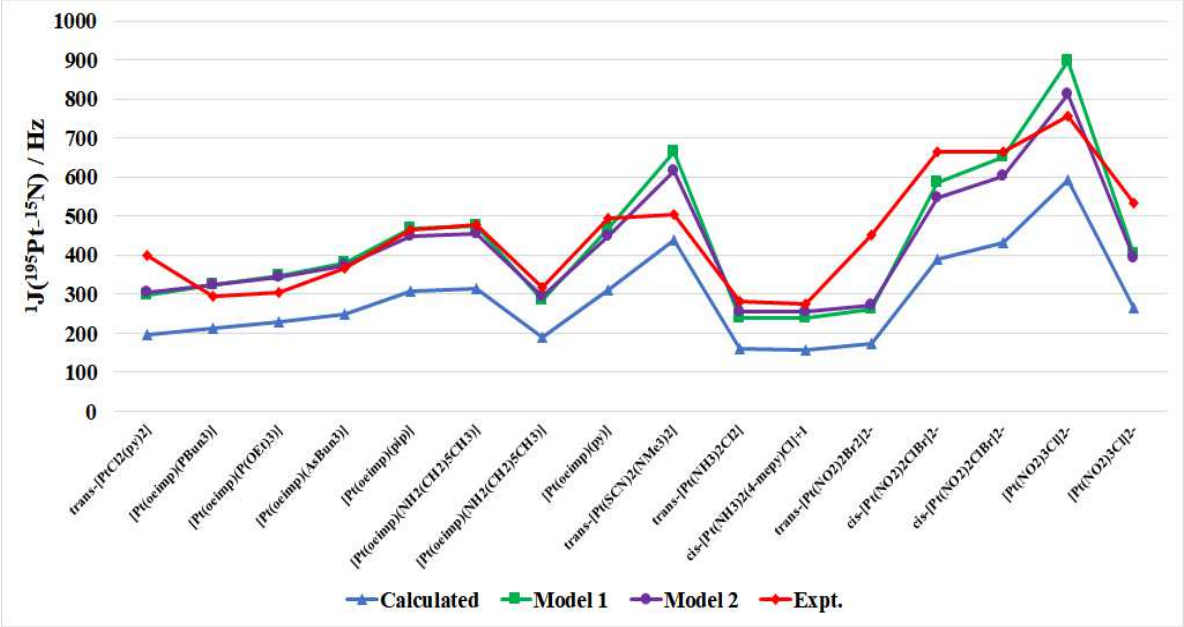

Reference: Own Author.

5 CONCLUDING REMARKS

The coupling constant, J, is a property of the NMR phenomenon and it helps to understand, characterize and develop reactional mechanisms, drugs and interactions between systems. Due to its sensibility and complexity, the study of protocol development and methodology are not widely studied for systems with heavy atoms. In this work 67 Pt(II) complexes with at least on nitrogen ligand, with 92 different J(Pt-N) coupling constants, were taken under study to develop a computational protocol for the calculation of the $^{1}J(^{195}Pt\text{-}^{15}N)$ coupling constant using a basis set that was first developed for the calculation of the chemical shift of the ^{195}Pt nuclide, the NMR-DKH basis set.

The initial proposed protocol was the same as the one developed by the creators of the basis set for the calculation of the ^{195}Pt chemical shift: PBEPBE/NMR-DKH/IEFPCM(UFF)//B3LYP/ LANL2DZ/def2-SVP/IEFPCM(UFF). This protocol yielded coupling constants with MAD of 105 Hz and MRD of 34.1%. From the 92 coupling constants, 82 presented underestimated value compared to their respective experimental value, whereas only 10 presented overestimated values. The behavior of the coupling constant was similar throughout the set of complexes, showing that the error was systematical. In order to try to understand and improve the protocol a set of four complexes was taken from the set of complexes in which a series of tests was performed. These tests aimed to improve the results and understand the behavior of the calculated coupling constant. Different protocols were tested on this test set where modifications on the NMR-DKH basis set were performed, as well as changes on the functionals and use of different basis sets, either for the ligand and metal, as well as just for the ligands. Tests were also performed on complexes with overestimated coupling constants to better understand this overestimation. And a last test was run by manually changing the Pt-N bond length to see how the coupling constant would vary with this change. The tests involving the modifications on the NMR-DKH basis set showed that addition of s functions with high exponent for the calculation of the contribution J^{FC} improved the results for the complexes with overestimated coupling constants. As for the functional tests, the functional M06 yielded slightly better results also for the overestimated complexes, decreasing the MRD from 51.6 to 50.7%. The results from the tests using different basis set for both metal and ligand were very unsatisfactory, showing that the results yielded with the NMR-DKH basis set were relatively satisfactory, though not ideal. The use of different basis set only for the ligands did not show any significative change. The tests with the overestimated complexes allowed to

conclude that the conformation of bulky ligands does not play a key role in the calculation of the coupling constant, and, also, the bulky phosphine and arsine ligands as well as isocyanate ligands may be involved in the overestimation of the coupling constants, though further analysis must be run to have more concrete details on how they influence the calculation. From the run tests a new protocol was proposed: M06/NMR-DKH(+mixed)/IEFPCM(UFF)//B3LYP/ LANL2DZ/def2-SVP/IEFPCM(UFF). This protocol was tested on all the 67 complexes. This new protocol proved to significantly improve the results for the overestimated complexes, whilst decreased the results for the underestimated constant. Taking only the overestimated constants, the MAD was 20 Hz and the MRD 14.2%. Since the overestimated complexes are minority in the working set of complexes, this protocol was abandoned. Due to the similarity on the behavior of the calculated coupling constants with the experimental ones, and, also, due to the majority, the underestimated constants were taken into two scaling methods in order to achieve better results. The two scaling models were constructed using a set of 82 experimental coupling constants and validated with an additional set of 16 coupling constants. In total, 71 distinct Pt(II) complexes were considered. Without scaling, the MAD and MRD of the underestimated constants were 119 Hz and 34.2%, respectively. This was significantly improved after scaling, providing absolute and relative deviations of 36 Hz and 10.4% when Model 2 is applied: ${}^{1}J_i^{scal.-2} = 1.278\ {}^{1}J_i^{calc.} + 51.129$. This result, added to our previous model to calculate ^{195}Pt chemical shift (PASCHOAL, 2016), stablishes a single-job computational protocol to explore Pt(II) complex NMR. The outcomes are published in the Chemical Physics Letters journal (CARVALHO, *et al*, 2020).

REFERENCES

ADAMO, Carlo; BARONE, Vincenzo. Exchange functionals with improved long-range behavior and adiabatic connection methods without adjustable parameters: The mPW and mPW1PW models. **The Journal Of Chemical Physics**, [s.l.], v. 108, n. 2, p.664-675, 8 jan. 1998. AIP Publishing.

ADAMO, Carlo; BARONE, Vincenzo. Toward reliable density functional methods without adjustable parameters: The PBE0 model. **The Journal Of Chemical Physics**, [s.l.], v. 110, n. 13, p.6158-6170, apr. 1999. AIP Publishing.

ANDERSON, Stephen J.; GOGGIN, Peter L.; GOODFELLOW, Robin J.. Study of the co-ordination behaviour of the thiocyanate and cyanate ions in some platinum(II) complexes by heteronuclear resonance spectroscopy. **Journal Of The Chemical Society, Dalton Transactions**, [s.l.], n. 19, p.1959-1964, 1976. Royal Society of Chemistry (RSC).

APPLETON, Trevor G.; HALL, John R.; RALPH, Stephen F.. Nitrogen-15 and platinum-195 NMR spectra of platinum ammine complexes: trans- and cis-influence series based on platinum-195-nitrogen-15 coupling constants and nitrogen-15 chemical shifts. **Inorganic Chemistry**, [s.l.], v. 24, n. 26, p.4685-4693, dec. 1985. American Chemical Society (ACS).

ARVANITIS, Georgia M.; WILK, Karen L.. Geometric Isomers of Platinum Coordination Compounds: An NMR Experiment for the Undergraduate Inorganic Chemistry Laboratory. **The Chemical Educator**, [s.l.], v. 2, n. 6, p.1-10, dec. 1997. Springer Science and Business Media LLC.

BECKE, Axel D.. Density-functional thermochemistry. III. The role of exact exchange. **The Journal Of Chemical Physics**, [s.l.], v. 98, n. 7, p.5648-5652, apr. 1993. AIP Publishing.

BECKE, Axel D.. Density-functional thermochemistry. IV. A new dynamical correlation functional and implications for exact-exchange mixing. **The Journal Of Chemical Physics**, [s.l.], v. 104, n. 3, p.1040-1046, 15 jan. 1996. AIP Publishing.

BERREDO, R.c. de; JORGE, F.e.. All-electron double zeta basis sets for platinum: Estimating scalar relativistic effects on platinum(II) anticancer drugs. **Journal Of Molecular Structure**: THEOCHEM, [s.l.], v. 961, n. 1-3, p.107-112, dec. 2010. Elsevier BV.

BJERKE, André. **Prinsessen spinner i berget**: dikt. Oslo: H. Aschehoug & Co, 1953.

BOYS, S. F.. Electronic wave functions - I. A general method of calculation for the stationary states of any molecular system. **Proceedings Of The Royal Society Of London. Series A. Mathematical And Physical Sciences**, [s.l.], v. 200, n. 1063, p.542-554, 22 feb. 1950. The Royal Society.

CARVALHO, J.; PASCHOAL, D.; GUERRA, C. Fonseca; SANTOS, H.f. dos. Nonrelativistic protocol for calculating the 1J(195Pt-15N) coupling constant in Pt(II)-complexes using all-electron Gaussian basis-set. **Chemical Physics Letters**, [s.l.], v. 745, p.137279-137286, apr. 2020. Elsevier BV.

CRAMER, Christopher J.. **Essentials of Computational Chemistry**: Theories and Models**.** 2. ed. [s. L.]: Wiley, 2004. 607 p.

DAVIDSON, Ernest R.. Comment on "Comment on Dunning's correlation-consistent basis sets". **Chemical Physics Letters**, [s.l.], v. 260, n. 3-4, p.514-518, sep. 1996. Elsevier BV.

DOS SANTOS, Hélio F.; ALMEIDA, Wagner B. de. MNDO/AM1/PM3 quantum mechanical semiempirical and molecular mechanics barriers to internal rotation: a comparative study. **Journal Of Molecular Structure**: THEOCHEM, [s.l.], v. 335, n. 1-3, p.129-139, may 1995. Elsevier BV.

DUARTE, Hélio Anderson. Índices de reatividade química a partir da teoria do funcional de densidade: formalismo e perspectivas. **Química Nova**, [s.l.], v. 24, n. 4, p.501-508, 2001.

DUNNING, Thom H.. Gaussian Basis Functions for Use in Molecular Calculations. I. Contraction of (9s5p) Atomic Basis Sets for the First-Row Atoms. **The Journal Of Chemical Physics**, [s.l.], v. 53, n. 7, p.2823-2833, oct. 1970. AIP Publishing.

DUNNING, Thom. H.. Gaussian Basis Functions for Use in Molecular Calculations. III. Contraction of (10s6p) Atomic Basis Sets for the First-Row Atoms. **The Journal Of Chemical Physics**, [s.l.], v. 55, n. 2, p.716-723, 15 jul. 1971. AIP Publishing.

DUNNING, Thom H.. Gaussian basis sets for use in correlated molecular calculations. I. The atoms boron through neon and hydrogen. **The Journal Of Chemical Physics**, [s.l.], v. 90, n. 2, p.1007-1023, 15 jan. 1989. AIP Publishing.

ERNZERHOF, Matthias; SCUSERIA, Gustavo E.. Assessment of the Perdew–Burke–Ernzerhof exchange-correlation functional. **The Journal Of Chemical Physics**, [s.l.], v. 110, n. 11, p.5029-5036, 15 mar. 1999. AIP Publishing.

Gaussian 09, Revision D.01 e A.02, FRISCH, M. J.; TRUCKS, G. W.; SCHLEGEL, H. B.; SCUSERIA, G. E.; ROBB, M. A.; CHEESEMAN, J. R.; SCALMANI, G.; BARONE, V.; MENNUCCI, B.; PETERSSON, G. A.; NAKATSUJI, H.; CARICATO, M.; LI, X.; HRATCHIAN, H. P.; IZMAYLOV, A. F.; BLOINO, J.; ZHENG, G.; SONNENBERG, J. L.; HADA, M.; EHARA, M.; TOYOTA, K.; FUKUDA, R.; HASEGAWA, J.; ISHIDA, M.; NAKAJIMA, T.; HONDA, Y.; KITAO, O.; NAKAI, H.; VREVEN, T.; MONTGOMERY, J. A., JR.; PERALTA, J. E.; OGLIARO, F.; BEARPARK, M.; HEYD, J. J.; BROTHERS, E.; KUDIN, K. N.; STAROVEROV, V. N.; KOBAYASHI, R.; NORMAND, J.; RAGHAVACHARI, K.; RENDELL, A.; BURANT, J. C.; IYENGAR, S. S.; TOMASI, J.; COSSI, M.; REGA, N.; MILLAM, J. M.; KLENE, M.; KNOX, J. E.; CROSS, J. B.; BAKKEN, V.; ADAMO, C.; JARAMILLO, J.; GOMPERTS, R.; STRATMANN, R. E.; YAZYEV, O.; AUSTIN, A. J.; CAMMI, R.; POMELLI, C.; OCHTERSKI, J. W.; MARTIN, R. L.; MOROKUMA, K.; ZAKRZEWSKI, V. G.; VOTH, G. A.; SALVADOR, P.; DANNENBERG, J. J.; DAPPRICH, S.; DANIELS, A. D.; FARKAS, Ö.; FORESMAN, J. B.; ORTIZ, J. V.; CIOSLOWSKI, J.; FOX, D. J. Gaussian, Inc., Wallingford CT, 2009.

GIL, Victor M. S.. **Ressonância magnética nuclear**: fundamentos, métodos e aplicações. Lisboa: Fundação Calouste Gulbenkian, 1987. 1012 p.

GUVEN, Adem et al. Cisplatin@US-tube carbon nanocapsules for enhanced chemotherapeutic delivery. **Biomaterials**, [s.l.], v. 33, n. 5, p.1455-1461, fev. 2012. Elsevier BV.

HAY, P. Jeffrey; WADT, Willard R.. Ab initio effective core potentials for molecular calculations. Potentials for the transition metal atoms Sc to Hg. **The Journal Of Chemical Physics**, [s.l.], v. 82, n. 1, p.270-283, jan. 1985. AIP Publishing.

HAY, P. Jeffrey; WADT, Willard R.. Ab initio effective core potentials for molecular calculations. Potentials for K to Au including the outermost core orbitals. **The Journal Of Chemical Physics**, [s.l.], v. 82, n. 1, p.299-310, jan. 1985. AIP Publishing.

HENDERSON, Thomas M. et al. Can short-range hybrids describe long-range-dependent properties? **The Journal Of Chemical Physics**, [s.l.], v. 131, n. 4, p.0441081-0441089, 28 jul. 2009. AIP Publishing.

HOHENBERG, P.; KOHN, W.. Inhomogeneous Electron Gas. **Physical Review**, [s.l.], v. 136, n. 3, p.B864-B871, 9 nov. 1964. American Physical Society (APS).

IIKURA, Hisayoshi et al. A long-range correction scheme for generalized-gradient-approximation exchange functionals. **The Journal Of Chemical Physics**, [s.l.], v. 115, n. 8, p.3540-3544, 22 aug. 2001. AIP Publishing.

JENSEN, Frank. **Introduction to Computational Chemistry.** 2. ed. Chichester: John Wiley & Sons, 2007.

JIN, Victor X.; TAN, Siew. I.; RANFORD, John D.. Platinum(II) triammine antitumour complexes: structure–activity relationship with guanosine 5′-monophosphate (5′-GMP). **Inorganica Chimica Acta**, [s.l.], v. 358, n. 3, p.677-686, feb. 2005. Elsevier BV.

KENDALL, Rick A.; DUNNING, Thom H.; HARRISON, Robert J.. Electron affinities of the first-row atoms revisited. Systematic basis sets and wave functions. **The Journal Of Chemical Physics**, [s.l.], v. 96, n. 9, p.6796-6806, may 1992. AIP Publishing.

KERRISON, S. John S.; SADLER, Peter J.. The trans influence in platinum chemistry. A platinum-195 nuclear magnetic resonance study of [15N]nitrito-, chloro-, and bromo-platinum-(II) and -(IV) complexes. **Journal Of The Chemical Society, Dalton Transactions**, [s.l.], n. 12, p.2363-2369, 1982. Royal Society of Chemistry (RSC).

KERRISON, S.john S.; SADLER, Peter J.. 195Pt NMR studies of platinum(II) dimethylsuphoxide complexes. **Inorganica Chimica Acta**, [s.l.], v. 104, n. 3, p.197-201, nov. 1985. Elsevier BV.

KOCH, Wolfram; HOLTHAUSEN, Max C.. **A Chemist's Guide to Density Functional Theory.** 2. ed. [s. L.]: Wiley-vch, 2001. 306 p.

KOHN, W.; SHAM, L. J.. Self-Consistent Equations Including Exchange and Correlation Effects. **Physical Review**, [s.l.], v. 140, n. 4, p.A1133-A1138, 1965. American Physical Society (APS).

LEE, Chengteh; YANG, Weitao; PARR, Robert G.. Development of the Colle-Salvetti correlation-energy formula into a functional of the electron density. **Physical Review B**, [s.l.], v. 37, n. 2, p.785-789, 15 jan. 1988. American Physical Society (APS).

LEVASON, W.; PLETCHER, D.. 195-Platinum Nuclear Magnetic Resonance Spectroscopy. **Platinum Metals Rev.**, Southampton, v. 37, n. 1, p.17-23, 01 jan. 1993.

LEVITT, Malcolm H.. **Spin Dynamics**: Basics of Nuclear Magnetic Resonance. 2. ed. Chichester: Wiley, 2008. 740 p.

LEWARS, Errol G.. **Computational Chemistry**: Introduction to the Theory and Applications of Molecular and Quantum Mechanics**.** 3. ed. New York: Springer, 2016.

MARDIROSSIAN, Narbe; HEAD-GORDON, Martin. Thirty years of density functional theory in computational chemistry: an overview and extensive assessment of 200 density functionals. **Molecular Physics**, [s.l.], v. 115, n. 19, p.2315-2372, 2017.

MCLEAN, A. D.; CHANDLER, G. S.. Contracted Gaussian basis sets for molecular calculations. I. Second row atoms, Z=11–18. **The Journal Of Chemical Physics**, [s.l.], v. 72, n. 10, p.5639-5648, 15 may 1980. AIP Publishing.

MIERTUŁ, S.; SCROCCO, E.; TOMASI, J.. Electrostatic interaction of a solute with a continuum. A direct utilizaion of AB initio molecular potentials for the prevision of solvent effects. **Chemical Physics**, [s.l.], v. 55, n. 1, p.117-129, feb. 1981. Elsevier BV.

MOTSCHI, Herbert; PREGOSIN, Paul S.; VENANZI, Luigi M.. 15N-NMR. and31P-NMR. Studies of palladium and platinum complexes. **Helvetica Chimica Acta**, [s.l.], v. 62, n. 3, p.667-677, 20 apr. 1979. Wiley.

MOTSCHI, H.; PREGOSIN, P.s.. Nitrogen-15 and platinum-195 nuclear magnetic resonance spectroscopy of platinum complexes. Schiff's base complexes of the tridentate ligand formed from ethanolamine-15N and salicylaldehyde. **Inorganica Chimica Acta**, [s.l.], v. 40, p.141-146, jan. 1980. Elsevier BV.

NORO, Takeshi; SEKIYA, Masahiro; KOGA, Toshikatsu. Sapporo-(DKH3)-nZP (n = D, T, Q) sets for the sixth period s-, d-, and p-block atoms. **Theoretical Chemistry Accounts**, [s.l.], v. 132, n. 5, p.1-5, 2 apr. 2013. Springer Science and Business Media LLC.

ONSAGER, Lars. Electric Moments of Molecules in Liquids. **Journal Of The American Chemical Society**, [s.l.], v. 58, n. 8, p.1486-1493, aug. 1936. American Chemical Society (ACS).

PARR, Robert G.; WEITAO, Yang. **Density-functional theory of atoms and molecules.** Oxford: Oxford University Press; Clarendon Press, 1994. 338 p.

PASCHOAL, D. et al. Predicting Pt-195 NMR chemical shift using new relativistic all-electron basis set. **Journal Of Computational Chemistry**, [s.l.], v. 37, n. 26, p.2360-2373, 11 aug. 2016. Wiley.

PERDEW, John P.; BURKE, Kieron; ERNZERHOF, Matthias. Generalized Gradient Approximation Made Simple. **Physical Review Letters**, [s.l.], v. 77, n. 18, p.3865-3868, 28 oct. 1996. American Physical Society (APS).

PERDEW, John P.; BURKE, Kieron; ERNZERHOF, Matthias. Generalized Gradient Approximation Made Simple. **Physical Review Letters**, [s.l.], v. 77, n. 18, p.3865-3868, 28 oct. 1996. American Physical Society (APS).

PERDEW, John P.; BURKE, Kieron; ERNZERHOF, Matthias. Generalized Gradient Approximation Made Simple [Phys. Rev. Lett. 77, 3865 (1996)]. **Physical Review Letters**, [s.l.], v. 78, n. 7, p.1396-1396, 17 feb. 1997. American Physical Society (APS).

PETERSON, Kirk A.; WOON, David E.; DUNNING, Thom H.. Benchmark calculations with correlated molecular wave functions. IV. The classical barrier height of the H+H2→H2+H reaction. **The Journal Of Chemical Physics**, [s.l.], v. 100, n. 10, p.7410-7415, 15 may 1994. AIP Publishing.

PLIEGO JUNIOR, Josefredo R.. Modelos contínuos do solvente: fundamentos. **Química Nova**, [s.l.], v. 29, n. 3, p.535-542, jun. 2006. FapUNIFESP (SciELO).

POEL, Henk van Der et al. A Comparative Study of Platinum Di (t-butyl) (15N2)diimine andtrans-[(PtCl2(N-ligand)PBu3)] complexes by195Pt-,31P- and15N-NMR. **Helvetica Chimica Acta**, [s.l.], v. 64, n. 4, p.1174-1182, 10 jun. 1981. Wiley.

PREGOSIN, P.s.. Platinum-195 nuclear magnetic resonance. **Coordination Chemistry Reviews**, [s.l.], v. 44, n. 2, p.247-291, jul. 1982. Elsevier BV.

QUINN, Charles M. **Computational Quantum Chemistry:** An Interactive Guide to Basis Set Theory. [s. L.]: Academic Press, 2002. 237 p.

RABI, I. I.. Space Quantization in a Gyrating Magnetic Field. **Physical Review**, [s.l.], v. 51, n. 8, p.652-654, 15 abr. 1937. American Physical Society (APS).

RAMSEY, Norman F.. Electron Coupled Interactions between Nuclear Spins in Molecules. **Physical Review**, [s.l.], v. 91, n. 2, p.303-307, 15 jul. 1953. American Physical Society (APS).

SCALMANI, Giovanni; FRISCH, Michael J.. Continuous surface charge polarizable continuum models of solvation. I. General formalism. **The Journal Of Chemical Physics**, [s.l.], v. 132, n. 11, p.1141101-11411015, 21 mar. 2010. AIP Publishing.

STAROVEROV, Viktor N. et al. Comparative assessment of a new nonempirical density functional: Molecules and hydrogen-bonded complexes. **The Journal Of Chemical Physics**, [s.l.], v. 119, n. 23, p.12129-12137, 15 dec. 2003. AIP Publishing.

STEPHENS, P. J. et al. Ab Initio Calculation of Vibrational Absorption and Circular Dichroism Spectra Using Density Functional Force Fields. **The Journal Of Physical Chemistry**, [s.l.], v. 98, n. 45, p.11623-11627, nov. 1994. American Chemical Society (ACS).

STILL, Brett M. et al. 195Pt NMR—theory and application. **Chem. Soc. Rev.**, [s.l.], v. 36, n. 4, p.665-686, 2007. Royal Society of Chemistry (RSC).

SUTTER, Kiplangat; TRUFLANDIER, Lionel A.; AUTSCHBACH, Jochen. NMR J-Coupling Constants in Cisplatin Derivatives Studied by Molecular Dynamics and Relativistic DFT. **Chemphyschem**, [s.l.], v. 12, n. 8, p.1448-1455, 4 mar. 2011. Wiley.

SUTTER, Kiplangat; AUTSCHBACH, Jochen. Computational Study and Molecular Orbital Analysis of NMR Shielding, Spin–Spin Coupling, and Electric Field Gradients of Azido Platinum Complexes. **Journal Of The American Chemical Society**, [s.l.], v. 134, n. 32, p.13374-13385, 3 aug. 2012. American Chemical Society (ACS).

TAO, Jianmin et al. Climbing the Density Functional Ladder: Nonempirical Meta–Generalized Gradient Approximation Designed for Molecules and Solids. **Physical Review Letters**, [s.l.], v. 91, n. 14, p.1464011-1464014, 30 sep. 2003. American Physical Society (APS).

TOMASI, Jacopo; PERSICO, Maurizio. Molecular Interactions in Solution: An Overview of Methods Based on Continuous Distributions of the Solvent. **Chemical Reviews**, [s.l.], v. 94, n. 7, p.2027-2094, nov. 1994. American Chemical Society (ACS).

VINJE, Jo; SLETTEN, Einar. NMR Spectroscopy of Anticancer Platinum Drugs. **Anti-cancer Agents In Medicinal Chemistry**, [s.l.], v. 7, n. 1, p.35-54, 1 jan. 2007. Bentham Science Publishers Ltd..

VYDROV, Oleg A. et al. Importance of short-range versus long-range Hartree-Fock exchange for the performance of hybrid density functionals. **The Journal Of Chemical Physics**, [s.l.], v. 125, n. 7, p.0741061-0741069, 21 aug. 2006. AIP Publishing.

VYDROV, Oleg A.; SCUSERIA, Gustavo E.. Assessment of a long-range corrected hybrid functional. **The Journal Of Chemical Physics**, [s.l.], v. 125, n. 23, p.2341091-2341099, 21 dec. 2006. AIP Publishing.

VYDROV, Oleg A.; SCUSERIA, Gustavo E.; PERDEW, John P.. Tests of functionals for systems with fractional electron number. **The Journal Of Chemical Physics**, [s.l.], v. 126, n. 15, p.1541091-1541099, 21 apr. 2007. AIP Publishing.

WEIGEND, Florian; AHLRICHS, Reinhart. Balanced basis sets of split valence, triple zeta valence and quadruple zeta valence quality for H to Rn: Design and assessment of accuracy. **Physical Chemistry Chemical Physics**, [s.l.], v. 7, n. 18, p.3297-3305, 2005. Royal Society of Chemistry (RSC).

WILSON, Angela K.; VAN MOURIK, Tanja; DUNNING, Thom H.. Gaussian basis sets for use in correlated molecular calculations. VI. Sextuple zeta correlation consistent basis sets for boron through neon. **Journal Of Molecular Structure**: THEOCHEM, [s.l.], v. 388, p.339-349, dec. 1996. Elsevier BV.

WOOD, Fred E.; BALCH, Alan L.. Natural abundance 195Pt nuclear magnetic resonance studies of some platinum(II) nitro complexes. **Inorganica Chimica Acta**, [s.l.], v. 76, p.63-64, jan. 1983. Elsevier BV.

WOON, David E.; DUNNING, Thom H.. Gaussian basis sets for use in correlated molecular calculations. III. The atoms aluminum through argon. **The Journal Of Chemical Physics**, [s.l.], v. 98, n. 2, p.1358-1371, 15 jan. 1993. AIP Publishing.

YANAI, Takeshi; TEW, David P; HANDY, Nicholas C. A new hybrid exchange–correlation functional using the Coulomb-attenuating method (CAM-B3LYP). **Chemical Physics Letters**, [s.l.], v. 393, n. 1-3, p.51-57, jul. 2004. Elsevier BV.

ZHAO, Yan; TRUHLAR, Donald G.. The M06 suite of density functionals for main group thermochemistry, thermochemical kinetics, noncovalent interactions, excited states, and transition elements: two new functionals and systematic testing of four M06-class functionals and 12 other functionals. **Theoretical Chemistry Accounts**, [s.l.], v. 120, n. 1-3, p.215-241, 12 jul. 2007. Springer Science and Business Media LLC.

APPENDIX A – THEORETICAL FORMALISM

A.1 BASIS SET

The basis set is a linear combination of a finite set of mathematical functions that describes an orbital. The type of the mathematical function used to build a basis set is important and two different types are commonly used in quantum mechanics: Slater Type Orbitals (STO) and Gaussian Type Orbitals (GTO) (JENSEN, 2007).

STOs have a general expression given as:

$$\phi_{\xi,n,l,m}(r,\theta,\varphi) = NY_{l,m}(\theta,\varphi)r^{n-1}e^{-\xi r} \quad \text{(A.1)}$$

Where N is a normalization constant and $Y_{l,m}$ are spherical harmonic functions. STOs yield very satisfactory results for mono and diatomic systems due to the exponential dependency on r, increasing the convergency as the number of functions are increased. Though, for polyatomic systems, the STO integrals cannot be analytically solved, making its use less appealing. To solve this, Boys (BOYS, 1950) proposed another type of orbitals: the GTO.

Differently from STOs, the GTOs are dependent on r^2 instead of r, as showed following:

$$\phi_{\xi,n,l,m}(r,\theta,\varphi) = NY_{l,m}(\theta,\varphi)r^{2n-2-l}e^{-\xi r^2} \quad \text{(A.2)}$$

This dependency on r^2 makes GTOs inferior than STOs. However, this inferiority can be solved by combining multiples gaussian functions, as showed in Fig. A.1, adapted from Quinn (2002):

Figure A.1. Combination of three gaussian functions to yield a 1s Slater function

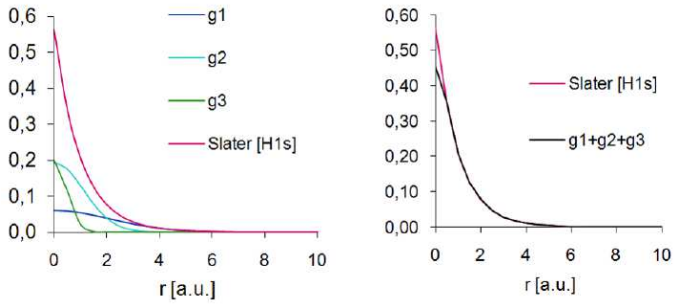

Reference: Adapted from QUINN, 2002.

On the left side we have three different gaussian functions (g1, g2 and g3) and a slater function for the 1s orbital for the hydrogen atom. The behavior of the three gaussian functions is poor compared to the slater function. It is clear that the gaussian functions decay faster than the slater function and, also, don't represent satisfactorily the nuclear region. If we combine the three gaussian functions, as showed on the right side, the behavior of the combined gaussian functions become much more similar to the slater function. It is fair to say, thus, that a slater type function can be modeled by three gaussian functions, yielding same precision as a STO, especially on the regions close and distant from the nucleus.

Basis sets can be classified according to their number of functions. The simplest type of basis set is called minimal basis set. In this type, the number of functions is the minimum to fully describe all electrons of the given atom in the ground state. For a first-row atom, for instance, it would require 1s functions. For the second row, 1s2s2px2py2pz, and so forth. Following the same idea, there are the n-zeta (NZ) basis set, where the number of functions is the double (DZ – double-zeta), triple (TZ – triple-zeta), and so forth (up until n=6) of the minimal basis set. Another classification of basis set consists in a mixture of the two previously presented, where the core electrons are described by minimal functions and the valence electrons by NZ functions. This classification is called valence basis set. The latter is important in calculations where the properties are highly dependent on the valence electrons. It is also important to mention the addition functions. There are two types of addition functions: polarization and diffuse functions. Polarization functions consist in functions with different angular momentum from the basis set in which they are being added to. It helps describing the distortion on the orbitals, important for the concept of chemical bond. As for the diffuse functions, they help describing systems in which the charge distribution is more diffuse than in the ground state. The diffuse functions increase the number of functions in the valence region and present lower exponent compared to the functions in the basis set.

The basis set plays a key role in quantum mechanics. The difficulty increases with the number of electrons in the system, giving that each one of them is described by a basis set. Many-electron systems can become handy to treat due to the number of integrals needed to be calculated, especially in heavy atoms, such as transition metals. We can divide the electrons in two regions: core and valence regions. In transition metals, the valence electrons are much fewer than the core ones. For most of molecular properties, the valence electrons are most important, since the outermost electrons are the ones who interact. In the cases where the core electrons aren't too important for the property calculation, there is an approximation largely employed that simplifies the calculation by substituting the core orbitals by pseudopotentials,

treating explicitly only the valence orbitals. This approximation is called Effective Core Potentials (ECP). The ECP is an effective potential, generally comprehending the first 60 electrons (60-electron ECP), that substitute the core operators, Coulomb and Exchange. This effective potential includes both core electrons interactions and core-valence electron interactions, the latter being done implicitly. The ECP approximation decreases considerably the calculation time, since the core electrons are no longer treated explicitly. ECP also recovers part of scalar relativistic effects. (HAY & WADT, 1985; HAY & WADT, 1985).

A.2 CONTINUOUS SOLVATION MODEL

The solvent effects can be of great importance in chemistry. When dealing with solution experimental data, the theoretical calculations must, somehow, mimic the solute-solvent interactions, especially when properties that are influenced by these interactions are being calculated. In this present work, the continuous solvation model was employed in all calculations.

Onsager (ONSAGER, 1936), in 1936, presented a model where the solvent was represented by a dielectric continuum and the solute, or the molecule being studied, was placed within a solvent cavity. The continuous models are based on Poisson equation that corelates the charge distribution, ρ, the electrostatic potential, ϕ, and the dielectric constant, ε:

$$\nabla^2(r) = -\frac{4\pi\rho(r)}{\varepsilon} \tag{A.3}$$

It is necessary, then, to model the cavity where the solute must fit. There are many different ways to model this cavity (TOMASI & PERSICO, 1994). An interesting approach is to use spherical and ellipsoidal cavities, due to their fairly simple mathematical solutions. That leads, though, to a certain inaccuracy, due to the fact that the cavities aren't spherically or ellipsoidally shaped. One way to correct this is to build spheres centered in the atoms, building a cavity coherent with the molecular shape. In this present work, the Polarizable Continuum Model (PCM) was employed to simulate the solvation model.

The PCM method was developed and presented by Tomasi and coworkers (MIERTUŠ; SCROCCO; TOMASI, 1981). In this method, the cavity is built by overlapping spheres centered in each atom. The sphere radius is specific for each atom (PLIEGO Jr., 2006). This sphere overlapping generates the molecular cavity, as exemplified in Fig. A.2, representing the cisplatin molecule and its cavity. This method presents some limitations. The solute-solvent interactions represented in this method are those to electrostatic origin. Any dynamic effects are neglected. Short-range interactions, such as hydrogen bond, van der Waals interaction and charge transference are not taken into consideration by utilizing the continuous solvation model (LEWARS, 2011). Furthermore, only the ground state of the solution is to be considered. This

continuous solvation model takes the solution as very dilute, since only one molecule of the solvent is placed in the solution, taken as the dielectric continuum.

It is worth mentioning that the solvent can also be treated explicitly, differently from what's described above. This method consists in placing the solvent molecules around the solute molecule (JENSEN, 2007). Advantages of this method is to represent both dynamism and short-range interactions. This method, though, is computationally expensive, since the number of atoms in the system is considerably increased, demanding more calculation steps. It becomes impractical, computationally-wise, to employ this method for large systems, especially those including heavy atoms.

Figure A.2. Cisplatin in a cavity of overlapping spheres contained in a continuum dielectric solvent

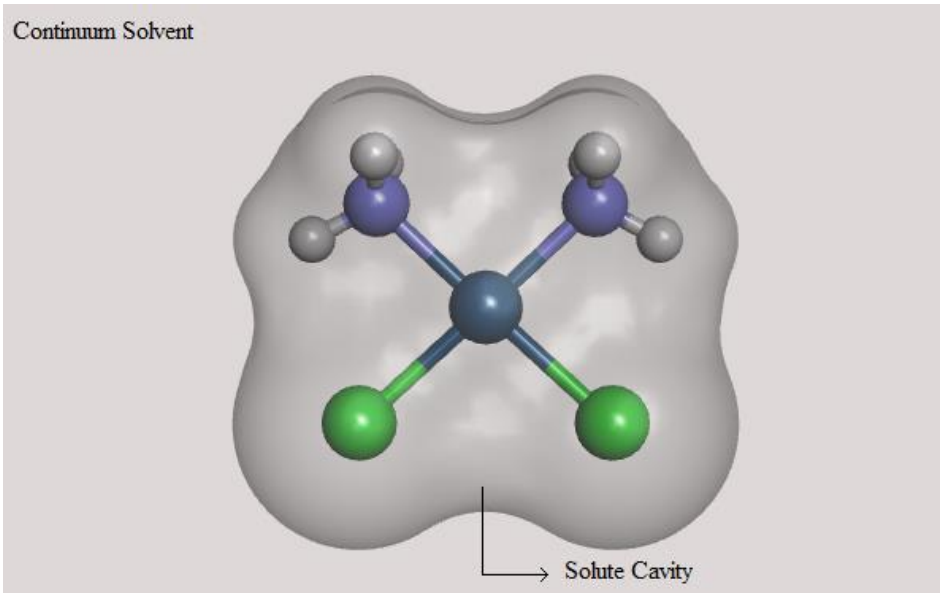

Reference: Own Author.

A.3. DENSITY FUNCTIONAL THEORY

The Density Functional Theory (DFT) is a widely used theory level in Computational Chemistry and it was first proposed by Hohenberg and Kohn in 1964 (HOHENBERG & KOHN, 1964). The DFT is based on the electronic density, ρ, and uses this property to calculate a number of atomic and molecular properties. The use of electronic density is mathematically more viable than the wave function, since the wave function has four different variables (x, y, z, spin) for each electron, whereas the electronic density is composed by only three variables for the entire system (x, y, z), decreasing drastically the number of variables to be taken into the calculation. Furthermore, it is possible to experimentally measure the electronic density, making the electronic density more concrete than the wave function, in terms of understanding it (LEWARS, 2011). The so-called DFT, as we known today, was based on two theorems proposed by Hohenberg and Kohn, and they will be presented following.

A.3.1. First Hohenberg-Kohn Theorem

The first theorem proposed by Hohenberg and Kohn is the essence of the DFT. It establishes that the total energy of a given system can be given as a functional of the electronic density (KOCH & HOLTHAUSEN, 2001):

$$E_o = E_o[\rho_o] \tag{A.4}$$

According to Hohenberg and Kohn, the external potential, υ(r), is given by the electronic density and this potential is produced by the atomic nuclei and by the electron number of the given system (N):

$$\int \rho(r)dr = N \tag{A.5}$$

This theorem predicts that there is a functional in which any molecular property can be calculated by. It, however, does not dictate what this functional is like.

A.3.2. Second Hohenberg-Kohn Theorem

The second theorem establishes the variational principle applied to DFT, i.e., the energy obtained by the electronic density functional is equal or higher than the exact energy (HOHENBERG & KOHN, 1964):

$$E_v(\rho_g) \geq E_o(\rho_o) \tag{A.6}$$

where ρ_g is the guess electronic density and $E_o(\rho_o)$ is the ground state exact energy, being ρ_o the exact electronic density.

The guess electronic density must meet two conditions: when integrate in all variables, the guess electronic density must be equal to the number of electrons of the given system:

$$\int \rho_g(r)dr = N \tag{A.7}$$

And the number of electrons per unit of volume cannot be negative:

$$\rho_g(r) \geq 0 \tag{A.8}$$

The universal functional is given by means of the kinetic and electron-electron repulsion operators, that do not change for any system with a given number of electrons and an external potential. Thus, the mathematical form of the universal function is given by:

$$F[\rho] = \langle \psi | \hat{T} + \hat{V}_e | \psi \rangle \tag{A.9}$$

where $\hat{T}$ is the kinetic energy operator and $\hat{V}_e$ is the electron-electron repulsion operator. The ground state energy of a many-electron system under a given external potential is:

$$E_\psi[\rho(r)] = \int v(r)\rho(r)dr + F[\rho] \tag{A.10}$$

A.3.3. Kohn-Sham Theory

We have seen so far that the energy, and thus other properties, can be expressed as a functional of the electronic density, but the functional itself has not been presented yet. In 1965, Kohn and Sham presented the first DFT method based on the two theorems from Hohenberg and Kohn. Kohn and Sham (KOHN & SHAM, 1965) introduced a new reference system for independent particles that do not interact with each other, coming up with the universal function G(r):

$$E_\rho[\rho] = G[\rho] + \frac{1}{2}\iint \frac{\rho(r)\rho(r')}{|r-r'|} + \int v(r)\rho(r)dr \tag{A.11}$$

where G[ρ] is given by:

$$G[\rho] = T_s[\rho] + E_{XC}[\rho] \tag{A.12}$$

being T_s the kinetic energy functional and E_{XC} the exchange-correlation functional that comprehends both electron-electron interactions (exchange and correlation), as well as residual part of the kinetic energy, given by $T[\rho] - T_s[\rho]$, where T[ρ] is the exact kinetic energy (DUARTE, 2001).

The kinetic energy can be achieved by a self-consistent method using a one-electron orbital:

$$T_s[\rho] = \sum_i^N \left\langle \psi_i \left| \frac{1}{2}\nabla^2 \right| \psi_i \right\rangle \tag{A.13}$$

These orbitals are eigenfunctions of the one-electron effective Kohn-Sham Hamiltonian (H_{KS}), as following:

$$\hat{H}_{KS} = -\frac{1}{2}\nabla^2 + v_{eff}(r) \tag{A.14}$$

where the effective potential, v_{eff}, is given by:

$$v_{eff}(r) = v(r) + \int \frac{\rho(r')}{|r - r'|} dr' + v_{XC}(r) = \frac{\delta E_{XC}[\rho]}{\delta \rho(r)} \quad \text{(A.15)}$$

The electronic density is given by means of the one-electron wave function:

$$\rho(r) = \sum_{i}^{N} |\psi_i(r)|^2 \quad \text{(A.16)}$$

The Kohn-Sham orbitals can, then, be obtained from the one-electron time-independent Schrödinger equation:

$$\left(\frac{1}{2}\nabla^2 + v_{eff}\right)\psi_i = \varepsilon_i \psi_i \quad \text{(A.17)}$$

Since the effective potential, v_{eff}, is dependent to the electronic density, the Kohn-Sham equations can be solved by a self-consistent method as showed in the flow chart in Fig. A.3 (CRAMER, 2004).

The hardest part of the DFT method is to determine the exchange-correlation functional, E_{XC}. Throughout the years and until nowadays different E_{XC} are developed based on the needs of the calculation, since most of functionals are validated by experimental data. The main difference between the many existent functionals lies in the ingredients used to build them. The main different types of functionals will be briefly presented following.

A.3.4 Local Density Approximation Functionals

The Local Density Approximation (LDA) (PARR; WEITAO, 1994) is the simplest type of functional. The only ingredient used to build the exchange-correlation functional is the one proposed by Hohenberg and Kohn: the electronic density. The functional is given by the following integration:

$$E_{XC}[\rho(r)] = \int \rho(r) e_{XC}[\rho(r)] dr \quad \text{(A.18)}$$

Figure A.3. Flow chart of the Kohn-Sham SCF procedure

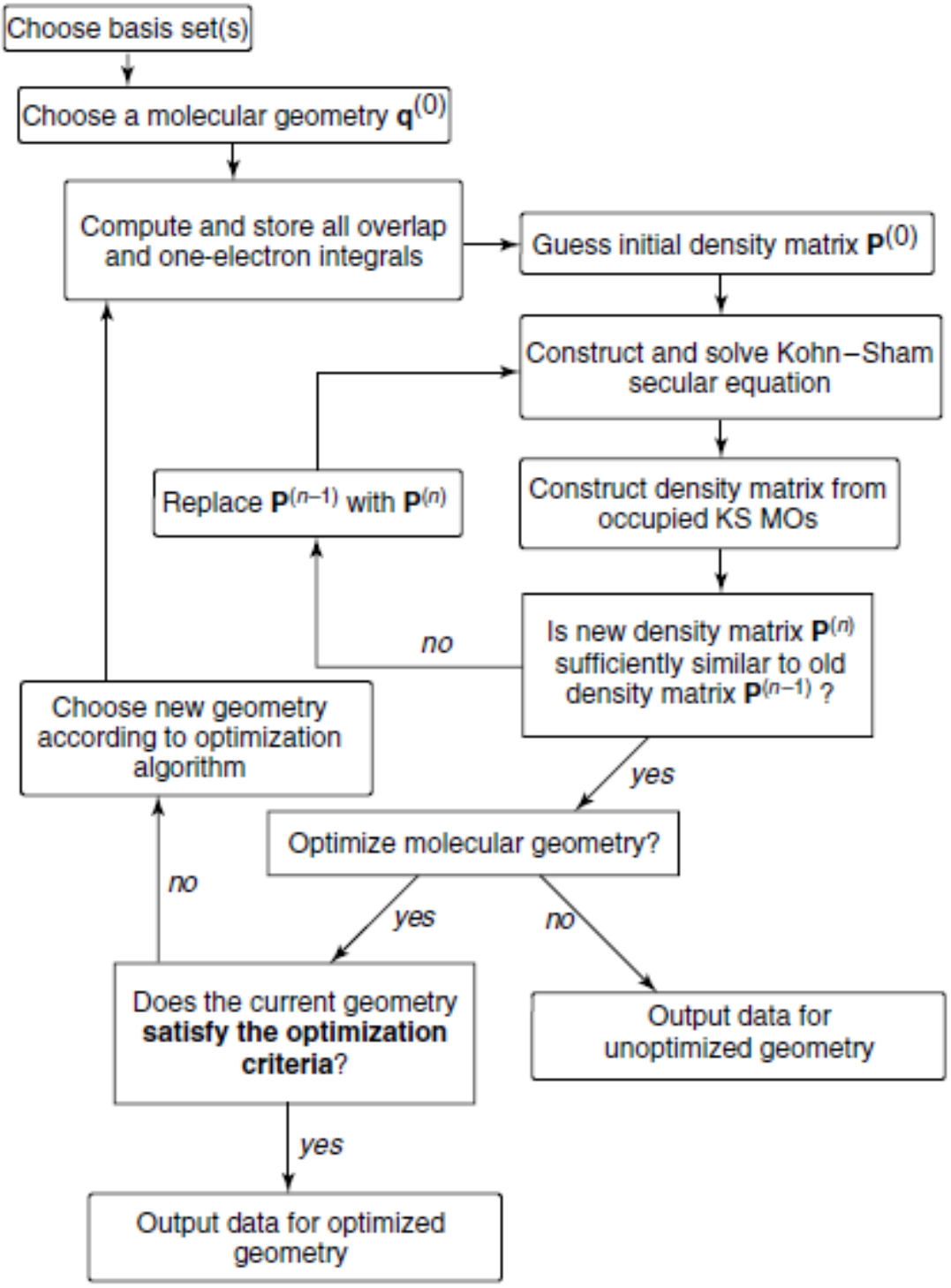

Reference: CRAMER, 2004.

The term e_{XC} corresponds to the exchange and correlation energy of a given uniform electron gas (UEG) with electronic density ρ at a given point r. This functional is accurate for an infinite UEG and treats the electronic density as homogeneous throughout the entire space. The LDA functional can be broadened into a more specific treatment, where the electrons of a given orbital are distinguished, treated here as α and β. This approach to the LDA functional is called Local Spin Density Approximation (LSDA). This treatment is efficient for system in which electrons are despaired, such as radical systems. If the system holds all electrons paired, the LSDA becomes the LDA, for there is no need to differentiate the spins, i.e. $\alpha = \beta$. There is no analytical form for the correlation functional, as for the exchange functional, it is given by means of the electronic density:

$$E_X^{LDA} = \sum_{\sigma}^{\alpha,\beta} \int e_{X,\sigma}^{UEG}\, d\vec{r} = -\frac{3}{2}\left(\frac{3}{4\pi}\right)^{\frac{1}{3}} \sum_{\sigma}^{\alpha,\beta} \rho_{\sigma}^{\frac{4}{3}} d\vec{r} \qquad \text{(A.19)}$$

This functional is very simple and sustains only accuracy for systems with approximately uniform density, which are very few. The lack of heterogeneity in the treatment of the electronic density gave rise to a new class of functionals called Generalized Gradient Approximation (GGA).

A.3.5. Generalized Gradient Approximation

In order to correct the systematic errors in LSDA due to inhomogeneities of the electronic density, a new ingredient was used to build functionals: the gradient of the electronic density, ∇ρ. Now, besides being dependent on the electronic density, the functional is also dependent on its gradient. This addition improved significantly the results of GGA functionals over the LSDA ones (MARDIROSSIAN; HEAD-GORDON, 2017). A generic GGA functional can be expressed by the following integration:

$$E_X^{GGA} = \sum_{\sigma}^{\alpha,\beta} \int e_{X,\sigma}^{UEG}\, g_{X,\sigma}^{GGA}\, d\vec{r} \qquad \text{(A.20)}$$

where the term g^{GGA} is called inhomogeneity correction factor (ICF) and it is responsible to enhance the exchange energy term, e^{UEG}. Beyond the addition of this new ingredient, it is also

possible to semi-empirically parametrize the GGA functionals, creating a new subclass of functionals, though most of the functionals are non-empirical. Some examples of non-empirical exchange-correlation functionals are: BP86, BLYP, PW91, revPBE, RPBE and PBEsol. And for the semi-empirical exchange-correlation functionals: HCTH/93, HCTH/120, HCTH/147 and HCTH/407.

A.3.6. Meta-Generalized Gradient Approximation

The meta-generalized gradient approximation (mGGA) (MARDIROSSIAN; HEAD-GORDON, 2017) will be the last class presented in this work, though other subclasses will be also in the scope of this session. For the mGGA class, two new ingredients are added in the functionals: the Laplacian of the density, $\nabla^2\rho$, and the kinetic energy density, τ_σ. The kinetic energy density is given by:

$$\tau_\sigma = \sum_{i}^{n,\sigma} \left|\phi_{i,\sigma}\right|^2 \tag{A.21}$$

These two new ingredients are correlated and, due to this correlation, most of functionals presents only one of them, though there are functionals that present both of them in the same functional. The correlation between these two entities is:

$$\tau_\sigma = \frac{\nabla^2\rho_\sigma}{2} - \sum_{i=1}^{n,\sigma} \phi_{i,\sigma}^{*}\,\vec{r}\nabla^2\phi_{i,\sigma}\vec{r} \tag{A.22}$$

The mGGA functionals, regardless of presenting more ingredients, do not take much longer in calculations than the GGA ones, yielding to better results in some times. The functional is expressed by a similar integration to the GGA one:

$$E_X^{mGGA} = \sum_{\sigma}^{\alpha,\beta} \int e_{X,\sigma}^{UEG}\, g_{X,\sigma}^{mGGA}\, d\vec{r} \tag{A.23}$$

Analogous to the GGA functionals, mGGA functionals can also be semi-empirically parametrize. Some examples of semi-empirical mGGA exchange-correlation functionals are:

M06-L, M11-L, MN12-L and MN15-L. As for the non-empirical ones: PKZB, TPSS, revTPSS, MS0, MS1, MS2, MS5, SCAN, BLOC and TM.

Despite the LSDA, GGA and mGGA classifications, these functionals can be grouped into other classes. Two of them will be covered, for they were employed in this work: Global Hybrid (GH) and Range-Separated Hybrid (RSH).

A.3.7. Global Hybrid Functionals

So far, both exchange and correlation functionals were set under the DFT scope. It is possible, however, to use part of the Hartree-Fock (HF) theory simultaneously with DFT. With this junction of theories, a new category of functional arises: the Global Hybrid functional (MARDIROSSIAN; HEAD-GORDON, 2017). Functionals that follow exclusively DFT are called pure functionals, while functionals that mix both DFT and HF are called global hybrid, or simply hybrid functionals. This hybridization of the functionals comes in handy with some difficulties arisen from the pure functionals, for instance, it helps correcting the self-interaction error (SIE).

From the HF theory, the exchange energy is given by:

$$\varepsilon_X = -\sum_{i=1}^{n}\sum_{j=1}^{n} K_{ij} \tag{A.24}$$

where K_{ij} is the exchange operator. If we apply the Eq. (A.24) to the Kohn-Sham orbitals, the HF exchange energy can be given as:

$$\varepsilon_X^{HF} = -\sum_{i=1}^{n}\sum_{j=1}^{n} \left\langle \psi_i^{KS}(1)\psi_j^{KS}(2)\left|\frac{1}{r_{ij}}\right|\psi_i^{KS}(2)\psi_j^{KS}(1)\right\rangle \tag{A.25}$$

Since the Slater determinant is an exact representation of the wave function in a reference system with non-interacting electrons, ε_X^{HF} becomes the exact exchange energy of such system with electronic density equivalent to the real density. Therefore, a general expression for a hybrid functional is:

$$E_{XC}^{GH} = c_x E_X^{HF} + (1 - c_x)E_X^{DFT} + E_C^{DFT} \tag{A.26}$$

where the coefficient c_x determines how much exact exchange energy is considered in the functional, varying from 0% (pure functional) to 100%. It is important to mention that either DFT exchange and correlation functionals can be given as a linear combination of different functionals, as long as the sum of the coefficients for the correlation functionals is equal to 1, as well as the sum of the coefficients for the DFT and HF exchange functionals is also equal to 1.

Global hybrid functionals can either present GGA or mGGA functionals, and present or not semi-empirical parameters in their functionals.

A.3.8. Range-Separated Hybrid Functionals

The last classification covered in this work is the Range-Separated Hybrid (RHS) (MARDIROSSIAN; HEAD-GORDON, 2017). All RSH functionals are also GH functionals, and they can be either GGA or mGGA functionals. In this class the exact exchange part, i.e. the HF exchange, is divided into two terms: a short-ranged and a long-ranged term (Eq. A.27). This separation benefits errors arisen from the long-ranged interelectronic behaviors. By separating the exact exchange part, the HF exchange percentage is increased with growth of long-ranged interelectronic interaction.

$$E_X^{HF} = E_{X,sr}^{HF} + E_{X,lr}^{HF} \tag{A.27}$$

The factor that dictates this range separation is called range parameter and is usually denoted by the Greek letter ω. The HF Coulomb operator for the short-ranged term is attenuated by the complementary error function, denoted as $erfc(\omega_{r_{12}})$, as for the long-ranged HF Coulomb operator, the attenuation comes from the error function, denoted as $erf(\omega_{r_{12}})$. A general representation for a RHS functional is:

$$E_{XC}^{RHS} = c_{x,sr}E_{X,sr}^{HF} + c_{x,lr}E_{X,lr}^{HF} + \left(1 - c_{x,sr}\right)E_{X,sr}^{DFT} + \left(1 - c_{x,lr}\right)E_{X,lr}^{DFT} + E_C^{DFT} \tag{A.28}$$

A.4. NUCLEAR MAGNETIC RESONANCE AND COUPLING CONSTANT

A.4.1. Nuclear Magnetic Resonance

This section was based on the theory presented in the books from Levitt (LEVITT, 2008) and Gil (2007).

The Nuclear Magnetic Resonance (NMR), as in every spectroscopy technique, corresponds to the interaction of matter with radiation. Specifically, in the NMR case, the nuclear magnetic transitions, ΔE, are of such order that the frequency, υ, of the radiation interacting with the nuclei is of the radiofrequency ones. The transitions obey the Bohr frequency condition:

$$|\Delta E| = h\nu \tag{A.29}$$

where h is the Planck constant.

These energy states, as every energy state, are quantized, as already predicted by Bohr, in 1913, before the development of Quantum Mechanics. In 1924 Pauli suggested the existence of a nuclear angular momentum in order to explain the hyperfine structure of atomic spectra. Since the nuclear movement is neglectable when compared with the atom as a whole, the nuclear angular momentum must arise differently from the angular momentum of the electrons. Indeed, only in 1928 Dirac established the theoretical fundament of the nuclear angular momentum, which took place at the Dirac Relativistic Quantum Mechanics. This angular momentum from particles was called spin angular momentum. Although a classic view from the spin angular momentum may give the impression that the particles rotates around its axis, it is a wrong interpretation of this property. The spin angular momentum is an intrinsic property of any particle and, differently from the classical angular momentum, does not come from motion, it simply exists.

The nuclear angular momentum can take but discrete values, as it is quantized, according to one of the Quantum Mechanics postulates. The nuclear angular momentum can be expressed by a quantum number: the nuclear spin quantum number, denoted by *I*. The total spin angular momentum of a given nucleus depends on the proton and neutron number. Nuclei with even number of protons and neutrons have a total spin angular momentum equals 0, $I = 0$. If the number of protons is odd but the number of neutrons is even, *I* assume an integer value.

Now, if the number of neutrons is odd, whether the number of protons is odd or even, I is a half-integer.

For a nucleus with I = ½, there are two spin functions, denoted here by α and β. When these spin functions are operated by the nuclear spin momentum operator, $\hat{a}$, they yield eigenvalues as following:

$$\langle\alpha|\hat{a}_z|\alpha\rangle = \frac{1}{2}\hbar$$
$$\langle\beta|\hat{a}_z|\beta\rangle = -\frac{1}{2}\hbar \tag{A.30}$$

where $\hbar$ is the reduced Planck constant and $\hat{a}_z$ the z-component of the spin angular momentum operator.

These two spin functions are normally degenerated. However, when exposed to an external magnetic field, they no longer are degenerated, creating a state with an energy gap between them. The loss of degenerate state creates an interaction between the external magnetic field and the magnetic momentum arisen from the nuclear spin (note that the magnetic momentum associated with the nuclear spin is, too, an intrinsic property of every particle). The relation between the angular (a) and magnetic (μ) spin momenta is given as following:

$$\mu = \gamma a \tag{A.31}$$

The gamma-letter is a constant very important in NMR and it is called gyromagnetic ratio. This constant is unique for each nuclide and can take either negative or positive values, the latter being more common.

This energy difference arisen from the exposition to an external magnetic field creates the condition to which the NMR occur, called resonance condition. Taking the Bohr frequency condition (Eq. A.28), when exposed to an external magnetic field and irradiated with certain radiation, the nuclide will absorb the radiation which frequency satisfies the Bohr frequency condition. This phenomenon is called Nuclear Magnetic Resonance. However, not all nuclides are active to the NMR phenomenon. It is necessary that the resonance condition exists for the phenomenon to happen. It is required that the total spin nuclear momentum is different from zero, i.e. nuclides with odd proton and/or neutron number are active to NMR, whereas nuclides with even proton number are inactive.

A.4.2. Coupling Constant

There are many different interactions within the scope of the NMR. The most common, and probably important, is the chemical shift, which is a property that measures how much a nuclide feels the external magnetic field. In this work, however, the property investigated was the coupling constant, that might be taken as the second most important property within the NMR phenomenon. The coupling constant is commonly denoted by the letter J and can also be found under the names of indirect dipole interaction or spin-spin coupling. The coupling constant measures how much a nuclide feels another nuclide (hence, coupling) through the electrons (or electronic density) around them. Specifically, in this work the coupling constant taken was the $^{1}J(^{195}Pt\text{-}^{15}N)$, which means order-1 coupling constant between the ^{195}Pt and ^{15}N nuclides. Order-1 coupling constants are the interaction between two nuclides that are connected through a chemical bond in a molecule.

The Hamiltonian of a system exposed to an external magnetic field is given by:

$$\hat{H} = \frac{(\hat{p} + eA)^2}{2m} + \hat{V}_{ne} + \hat{V}_{ee} \tag{A.32}$$

Where first term corresponds to the kinetic energy, the second to the nucleus-electron interaction and the latter the electron-electron interaction. In this expression $\hat{p}$ is the linear moment, e is the elementary charge and A is the vector potential defined as:

$$A(r_i) = \frac{\mu_0}{4\pi} \sum_N \frac{\mu_N \times r_{iN}}{r_{iN}^3} \tag{A.33}$$

being μ_0 the magnetic vacuum permeability, μ_N the magnetic moment of nucleus N and r_{iN} the position of electron i to the nucleus N.

According to the Ramsey theory for nuclear spin coupling, there are three mechanism contributions for the coupling constant: spin-orbit, dipole-dipole and Fermi contact (RAMSEY, 1953). When expanded, the three mechanisms appear in the Hamiltonian, and they are treated as perturbation to the system.

(a) Spin-orbit mechanism

This coupling mechanism arises from the interaction between the orbital movement of the electrons with the nuclear magnetic moments. The nuclear magnetic moment of nucleus A generates currents that create a magnetic field at the nucleus of nucleus B. The sense of these currents depends on the spin orientation of the nucleus creating them, in this case, nuclide A. The Hamiltonian of this interaction is given by:

$$\widehat{H}_{SO} = \frac{\mu_0}{4\pi}\beta h \sum_N \sum_i \gamma_N \frac{L_{iN} I_N}{r_{iN}^3} \tag{A.34}$$

where β is the Bohr magneton constant, γ_N the gyromagnetic ration of nuclide N with nuclear spin I and L_{iN} is the angular moment of electron i in relation to nucleus N. This contribution can be divided into diamagnetic and paramagnetic contributions.

(b) Dipole-dipole mechanism

This interaction occurs between nuclear magnetic moments of nuclei and spin magnetic moment of electrons. The interaction between the two magnetic dipoles (hence dipole-dipole interaction) makes the nuclear magnetic moment of nucleus A generate a polarization on the electronic spins around it. The electronic spins interact likewise with nucleus B. Note that for the mean contribution of s-electrons of nucleus A is zero for the given nucleus due to its spherical symmetry. Since orbitals p,d and f aren't spherical shaped, they contribute for this interaction mechanism. The Hamiltonian for the dipole-dipole mechanism is given by:

$$\widehat{H}_{DD} = \frac{\mu_0}{4\pi^2}\beta h \sum_N \sum_i \gamma_N \left[\frac{3(S_i r_{iN})(I_N r_{iN})}{r_{iN}^5} - \frac{S_i I_N}{r_{iN}^3}\right] \tag{A.35}$$

where S_i is the spin angular momentum of electron i.

(c) Fermi contact mechanism

This mechanism arises from the "contact" interaction between the nuclear spins and electrons s. The term was proposed by Fermi when explaining the hyperfine structure in atomic spectra. Given a nucleus A, the s electrons belonging to this nuclide present spins anti-parallel to this magnetic nucleus. By means of coupling and exchange, this s electron from nuclide A

polarizes the spin of a s electron from nuclide B. This polarized s electron from nuclide B will try to align anti-parallelly with the s electron from nuclide A, generating the coupling to happen. This mechanism requires that the electron have high probability to be found near the nucleus (hence contact mechanism), causing the s electrons to be the ones involved in this type of mechanism. This mechanism is the one that contributes the most for the coupling constant and some calculations neglect, sometimes, other contributions in order to decrease the calculation time and cost. The Hamiltonian of this mechanism is given by:

$$\widehat{H}_{FC} = \frac{2\mu_0}{3\pi}\beta h \sum_N \sum_i \gamma_N \, \delta(r_{iN}) S_i I_N \tag{A.36}$$

being $\delta(r_{iN})$ the Dirac delta function:

$$\begin{aligned} \delta(r_{iN}) &= 1 \qquad if\ r_{iN} = 0 \\ \delta(r_{iN}) &= 0 \qquad if\ r_{iN} = 1 \end{aligned} \tag{A.37}$$

The perturbated Hamiltonian can be written as a sum of the Hamiltonian of the three mechanisms:

$$\widehat{H}' = \widehat{H}_{SO} + \widehat{H}_{DD} + \widehat{H}_{FC} \tag{A.38}$$

For the ground state, only the first-order term is considered, and the energy can be obtained from the following equation:

$$E' = \langle \psi_0 | \widehat{H}' | \psi_0 \rangle \tag{A.39}$$

From the eigenvalues, the coupling constant can be obtained by partially deriving the energy with respect to nucleus A and B nuclear spin:

$$J_{AB} = \frac{1}{h} \frac{\partial^2 E}{\partial I_A \partial I_B} \tag{A.40}$$